

Defining 3-dimensional marine provinces with phytoplankton compositions

Rafael Catoia Pulgrossi^{*1}, Nathan L R Williams ^{†2}, Yubin Raut^{‡3}, Jed Fuhrman^{§2}, and Sangwon Hyun^{*¶1}

¹*Department of Statistics, University of California, Santa Cruz*

²*Department of Biological Sciences, University of Southern California*

³*Earth, Atmosphere and Planetary Sciences, Massachusetts Institute of Technology*

December 10, 2025

*rcatoia@ucsc.edu
 †nathanwi@ucsc.com
 ‡yubin89@mit.edu
 §fuhrman@usc.edu
 ¶sangwonh@ucsc.edu

Abstract

Marine provinces rarely include fine-resolution biological data, and are often defined spatially across only latitude and longitude. Therefore, we aimed to determine how phytoplankton distributions define marine provinces across 3-dimensions (i.e., latitude, longitude, and depth). To do this, we developed a new algorithm called **bioprovince** which can be applied to compositional biological data. The algorithm first clusters compositional samples to identify spatially coherent groups of samples, then makes flexible province predictions in the broader 3d spatial grid based on environmental similarity. We applied **bioprovince** to phytoplankton Amplicon Sequencing Variants (ASVs) from five, depth-resolved ocean transects spanning north-south in the Pacific Ocean. In the surface layer of the ocean, our method agreed well with traditional Longhurst provinces. In some cases, the method revealed that with more granular taxonomic resolution afforded by ASVs, traditional Longhurst provinces were divided into smaller zones, mainly due to differences in the composition of *Prochlorococcus* ecotypes. One of the major advances of this method is its ability to incorporate a third dimension, depth. Indeed, our analysis found significant depth-wise partitions throughout the Pacific with remarkable agreement in the equatorial region with the base of the euphotic zone. In contrast, the Antarctic Longhurst province showed vertical homogeneity in ASV compositions, with our 3-dimensional bioprovinces extending with no division from the surface down to aphotic depth. Our algorithm's ability to delineate 3-dimensional bioprovinces will enable scientists to discover new ecological interpretations of marine phytoplankton ecology and biogeography. Furthermore, as compositional biological data inherently exists in three spatial dimensions in nature, bioprovince is broadly applicable beyond marine plankton, offering a more holistic perspective on biological provinces across diverse environments.

Keywords: *Clustering, Amplicon Sequence Variant, Marine Provinces, Global Plankton Survey, GRUMP*

1 Introduction

Partitioning and delineating marine areas into distinct regions directly enables a better understanding of the distribution of organisms and ecosystem processes. These regions are generally made by dividing the ocean into coherent and non-overlapping regions in space and are often referred to as marine provinces, biogeographic realms, seascapes, or ecoregions [1, 2, 3, 4]. Coherent delineation of ocean provinces helps us better understand global-scale biogeochemical processes (e.g., primary production [5, 6]), microbial distribution and diversity [7, 8, 9], assess fishery biomass and global ocean colour trends [10, 11], and assist with validation of larger scale ocean biogeochemistry general circulation models [12, 13]. There have been numerous efforts to define oceanic provinces, but much of the foundational work drew on globally distributed and seasonally varying ocean properties, such as chlorophyll concentration and parameters of the photosynthesis and light relationship throughout the water column, to partition primary production estimates into secondary compartments of 57 biogeochemical provinces nested within four primary pelagic biomes: Polar, Westerlies, Trade Winds, and Coastal [14, 15].

Longhurst [16] transformed the original province concept into a comprehensive biogeographical framework by systematically integrating a wide range of oceanographic parameters—including water column structure, nutrient availability, plankton community composition, and large-scale circulation patterns. Rather than relying solely on surface properties like chlorophyll or irradiance, Longhurst [16] incorporated data from hydrographic sections, climatological atlases, and ecological surveys to align province boundaries with functionally distinct oceanic regions. These refinements anchored the provinces not just in satellite observables but in ecological and physical processes, establishing a globally coherent system that reflects the dynamic coupling between ocean physics, biogeochemistry, and plankton ecology. Other studies have also aimed to objectively improve on these oceanographic boundaries by investigating their dynamic nature [17, 18, 19, 4] and integrating higher trophic organisms [2, 3]. More recent efforts have also sought to improve on these provinces by partitioning the deeper ocean layers such as the mesopelagic zone [20] or by incorporating more highly resolved phytoplankton biogeography [21].

With the advent of more affordable molecular technology and sequencing platforms, there is a proliferation of global ocean plankton surveys which provide scientists with incredible insight into the vast taxonomic and functional diversity of *in situ* marine plankton compositions [22, 23, 24, 25]. These datasets contain marine plankton relative abundances from the global ocean across a wide range of latitudes, longitudes, and depth, providing useful data that can be incorporated into ocean province boundary estimates. One notable related work [26] grouped prokaryotes together into ‘modules’ using co-occurrence networks, and investigated the spatial distribution of these modules. However, to our knowledge, no effort to date has (1) incorporated biological distribution of plankton at a molecular level with taxonomic granularity and (2) across depth in concert with abiotic environmental parameters into determining these provinces and oceanographic boundaries.

In this manuscript, we have developed a novel **bioprovince** algorithm (and accompanying open-source R software), which enables estimates of three-dimensional provinces extending across latitude, longitude, and depth in the ocean, primarily based on biological compositions of organisms. This method, which directly clusters biological samples and predicts spatial provinces, uses statistical and machine learning techniques in a pipeline with the major components being *objective*, in the sense that the key hyperparameters can be tuned from the data. This is highly preferable to a method that requires *subjective* choices from the data analyst, and ensures that the analysis results are reproducible. Consequently, the bioprovince framework is broadly applicable to any compositional dataset, such as those generated from metabarcoding, that is observed over space and is paired with associated abiotic metadata.

In order to prove the utility of our method, we applied it to compositional microbial phytoplankton data, which we sourced from the Global rRNA Universal Metabarcoding Plankton database (GRUMP) [27]. This dataset consists of sequenced DNA, which once bioinformatically processed, produce Amplicon Sequence Variances (ASVs). Each ASV or “DNA tag” is unique and belongs to a plankton species. The gene abundance or counts of each ASV in the GRUMP dataset are first transformed into relative abundances, based on our view that the relative abundance reflects the community mix of microbe species in the ocean. Off-the-shelf clustering methodology is usually not suitable for simply applying to compositional data, as most clustering methods assume a normal, Euclidean geometry of the data. Also importantly, clustering ASV samples with off-the-shelf clustering methods does not guarantee that spatially coherent clusters of samples

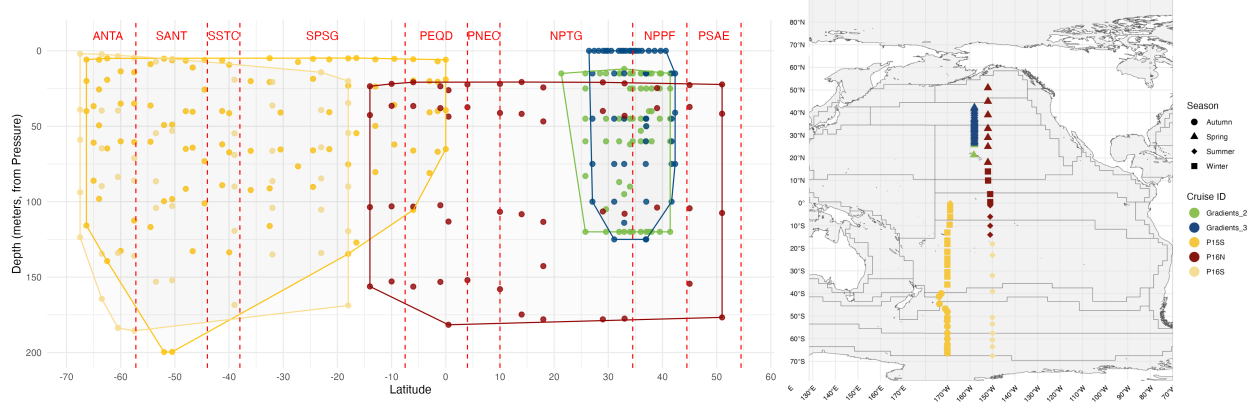


Figure 1: *Map of samples in space (latitude, longitude, and depth). There is heavy overlap between the cruises’ latitude-depth coverage. The two types of cruises (P15S, P16S, P16N compared to Gradients 2 and 3) differ greatly in their sampling. Note that we include data from 200m or above, which includes samples from below the euphotic zone.*

or provinces emerge. Our method incorporates spatially homogeneous clusters explicitly, and performs province predictions on a fine grid based on abiotic similarity. In our manuscript, we have made the following contributions:

1. We have developed an objective pipeline (**bioprovince**) for estimating ocean provinces across latitude-depth given ASV compositions and simple abiotic data (temperature and salinity).
2. We have developed methodology for tuning the main hyperparameters of our method. (Section 2)
3. We have applied our method to compositional phytoplankton ASV data from five cruises that encompass north-south transects in the Pacific Ocean across 14 years.

Our pipeline for clustering of biological data (the **biocluster** function) and province predictions on a spatial grid (the **bioprovince** function) are freely available as an R package, on github <https://github.com/sangwon-hyun/bioprovince-project>.

2 Material and Methods

2.1 Data

For our analysis, we used the “Global rRNA Universal Metabarcoding Plankton” (GRUMP) database version 1.3.5 [27]. GRUMP consists of 1,194 samples that were collected between 2003 and 2020 and cover extensive latitudinal and longitudinal transects, as well as depth profiles in all major ocean basins. Two significant factors make these data “universal”. The first is that the samples are not fractionated, meaning microbes from all size fractions are collected on the same filter during the sampling process. The second is that the DNA is sequenced using a universal primer pair, which captures all three domains of life. This means that the relative abundance data between all organisms and all samples within the dataset are comparable.

For this study, we used samples from five different cruises that latitudinally transected the Pacific Ocean. These cruises included the P15S cruise, which occurred in 2016, the P16S cruise in 2005, the P16N cruise in 2006, the Gradients 2 cruise in 2017, and the Gradients 3 cruise in 2019 (Figure 1). These cruises span the equatorial to high-latitude Pacific and were conducted in different years and seasons, providing a rich set of spatiotemporal contexts for evaluating community structure. Two of these cruises, P15S and P16S - offset by ~ 20 degrees longitude, traversed a vertical latitudinal transect from around the equatorial Pacific down into the highly productive waters of the Southern Ocean, but took place more than a decade apart (P16S in 2005, P15S in 2016). The other three cruises (P16N, Gradients 2, Gradients 3) transected the North Pacific Ocean at various spatial scales, spanning from the equator to $\sim 50^\circ\text{N}$ and were also taken multiple years apart

(P16N in 2006, Gradients 2 in 2017, Gradients 3 in 2018). The two SCOPE-Gradients cruises provide much smaller spatial coverage north of Hawaii, although at a much higher sampling frequency across the North Pacific Transition Zone (NPTZ) which is a significant ecological region separating the warmer, oligotrophic gyre and colder, more nutrient rich subarctic gyre [28]. It also differs from the GO-SHIP cruises in that a bidirectional transect is conducted so that the same latitudinal region is sampled twice separated over the course of about two weeks.

Seasonal differences across cruises further contribute to variability in community structure. Gradients 2 (May and June 2017) and 3 (April 2019) were conducted two years apart during overlapping seasons in the boreal spring (and also transition to early-summer), when there is often an uptick in phytoplankton productivity across the NPTZ, but strong environmental gradients (e.g., chlorophyll-*a* fronts, sea surface temperature, nutrients) shift seasonally [28]. The two P16 research expeditions, P16S and P16N, were also conducted during similar months, January - March, in consecutive years (2005 and 2006, respectively). However, due to their sampling locations spanning both hemispheres, they covered different seasonal contexts: P16S occurred during the austral summer, while P16N captured the austral summer south of the equator and a transition from boreal late-winter to early-spring north of the equator. The remaining cruise P15S, despite overlapping with P16S/N across similar regions south of the equator, was conducted about a decade later from April - June 2016, and captures the austral transition from autumn into winter.

Seawater was collected with niskin bottles at each station and then filtered through a 0.22-um filter that captures the entire microbial planktonic community, except for free-living viruses. The cells on this filter were then lysed to remove DNA from them, and then this DNA was purified for sequencing. Relative abundance information was generated by amplifying DNA with PCR using the 515FY, 926R universal rRNA gene primer pair [29] that amplify 16S (prokaryotic and chloroplast) and 18S (eukaryotic) ribosomal RNA. For this study, we used relative abundance values in the GRUMP column 'Corrected Sequence Counts'. These counts are corrected based off an essential downstream bioinformatic correction, as well as a sequencing biased against the longer 18S sequences compared to the shorter 16S sequences. For full details on sample processing, amplification, sequencing and bioinformatic pipeline, please see [24]. To assess the applicability of this statistical framework, we wanted to work with a digestible subset of the GRUMP data, which includes the three major plankton realms (i.e., bacterioplankton, phytoplankton, zooplankton). Phytoplankton are the major primary producers in the ocean ecosystem and have a profound impact on global biogeochemical cycles, supplying roughly half the oxygen in our atmosphere [30, 31]. Additionally, their roles and contributions in the ocean ecosystem are a primary component of classical Longhurst provinces and therefore, to stay consistent with our application of this algorithm, we also focused our efforts on the phytoplankton community in GRUMP.

This phytoplankton community was defined from ASV data as a combination of select Cyanobacteria and eukaryotic taxa inferred from chloroplast 16S sequences. The cyanobacterial component includes some of the smallest and most abundant photosynthetic organisms, such as *Prochlorococcus* and *Synechococcus*, as well as common nitrogen-fixing taxa (diazotrophs) such as (e.g., *Trichodesmium*, *Crocospaera*). Eukaryotic phytoplankton were identified based on chloroplast 16S sequences, indicative of their photosynthetic potential, with several major lineages excluded from the analysis. Specifically, sequences affiliated with macroalgae (e.g., Rhodophyta-red seaweeds), groups that commonly include kleptoplasts and photosymbionts (e.g., Rhizaria, Excavata), and Alveolata (which broadly include mixotrophic lineages in addition to kleptoplasty and photosymbioses) [32]. Notably, even though many dinoflagellates can be important constituents of the phytoplankton community, this group has lost most of the chloroplast genes [33] and therefore, is not very well captured in this sequence fraction of the dataset. Also, while dinoflagellates are well represented in the nuclear (18S) fraction of the GRUMP database, we are unable to tease apart their trophic strategy, which includes heterotrophy and mixotrophy, so they were excluded from this data analysis.

2.2 bioprovince Algorithm

Our proposed method, which we coin **bioprovince** algorithm, first creates geographically coherent clusters of compositional samples, then defines provinces in latitude and depth according to their agreement with the original samples' cluster memberships as well as their abiotic factors. Our method proceeds in three sequential steps:

Step 1. Form a pairwise distance matrix of samples. Each distance is a convex combination of (1) biological

distance between the two compositions, and (2) spatial distances between the sample's location.

Step 2. Use agglomerative hierarchical clustering to assign cluster memberships to the samples. We call Step 1 & 2 the **biocluster** algorithm.

Step 3. On a fine set of spatial gridpoints, use a *localized* nearest neighbor classification using abiotic factors.

Data analysts who wish to cluster samples can apply **biocluster** in Step 1-2. Those who wish to further constrain the spatial grid to define novel provinces should proceed to Step 3. We describe each step in detail next.

Step 1: Form pairwise distance matrix. Denote the compositional dataset as $\{\mathbf{p}_i\}_{i=1,\dots,n}$, where \mathbf{p}_i is a vector containing d microbial compositions observed at the i -th sample. Form pairwise biological distance matrix $D_{\text{bio}} \in \mathbb{R}^{n \times n}$ of the n samples using an *Aitchinson* distance [34] of the n compositions \mathbf{p}_i (for $i = 1, \dots, n$), so that the (i_1, i_2) -th entry $D_{\text{bio}}[i_1, i_2]$ is:

$$D_{\text{bio}}[i_1, i_2] = d_{\text{Aitchinson}}(\mathbf{p}_{i_1}, \mathbf{p}_{i_2}). \quad (1)$$

The Aitchison distance between two d -dimensional compositional vectors $\mathbf{p} = (\mathbf{p}_{[l]})_{l=1,\dots,d}$ and $\mathbf{q} = (\mathbf{q}_{[l]})_{l=1,\dots,d}$:

$$d_{\text{Aitchinson}}(\mathbf{p}, \mathbf{q}) = \sqrt{\sum_{l=1}^d \left(\ln \frac{\mathbf{p}_{[l]}}{g(\mathbf{p})} - \ln \frac{\mathbf{q}_{[l]}}{g(\mathbf{q})} \right)^2}, \quad (2)$$

where $g(\mathbf{x}) = \sqrt[d]{\prod_{l=1}^d \mathbf{x}_{[l]}}$ of vector $\mathbf{x} = (\mathbf{x}_l)_{l=1,\dots,d}$ is the geometric mean of its entries.

Also, denoting as $\text{lat}(\text{sample } i)$ and $\text{depth}(\text{sample } i)$ the latitude and depth of sample i , form the spatial distance matrix:

$$D_{\text{spatial}}[i_1, i_2] = \sqrt{r^2 \cdot (\text{lat}(\text{sample } i_1) - \text{lat}(\text{sample } i_2))^2 + (\text{depth}(\text{sample } i_1) - \text{depth}(\text{sample } i_2))^2}. \quad (3)$$

Next, take a convex combination of D_{bio} and D_{spatial} as follows (denoting as $h()$ the scaling operation that divides the columns of a matrix by its operator norm):

$$D_{\alpha} = (1 - \alpha) \cdot h(D_{\text{bio}}) + \alpha \cdot h(D_{\text{spatial}}). \quad (4)$$

for some fixed hyperparameter $0 \leq \alpha \leq 1$.

We note that an existing method ClustGeo [35] takes a similar approach to clustering spatial data. However, step 1 of our method is specialized for the application of marine microbe compositions, since the biological distances D_{bio} are Aitchison distances of compositional data, and the spatial distances – in latitude and depth – require additional care to determine the relative importance (r) of the two. We suggest a novel data-driven tuning strategy for the various hyperparameters (α , r , and K), described shortly in Section 2.4.

Step 2: Cluster the samples. Using the pairwise distance matrix D from (4), perform agglomerative hierarchical clustering [36] to obtain cluster memberships for each of the n compositions. Agglomerative hierarchical clustering is a bottom-up approach, starting with n distinct clusters, combining the two that have the smallest pairwise distances, then successively merging *hierarchically* using a linkage function between *groups* until K groups emerge. We opt for the Ward linkage function [37].

Step 3: Localized nearest neighbor prediction of memberships on a grid. Take a B -sized fine grid of spatial locations, indexed by j in 1 through B . For each of these spatial grid points j , find the k most similar samples according to *abiotic* conditions. Specifically, take the abiotic similarity between grid point j and sample i to be:

$$\sqrt{(\text{temperature}(\text{grid } j) - \text{temperature}(\text{sample } i))^2 + (\text{salinity}(\text{grid } j) - \text{salinity}(\text{sample } i))^2},$$

the ℓ_2 difference between temperature and salinity measurements – both linearly rescaled to be between zero and one. Next, take the estimated cluster memberships of these k closest samples that are *also* within the k closest in space, where spatial distance is defined as before in (3):

$$\sqrt{r^2 \cdot (\text{lat}(\text{grid } j) - \text{lat}(\text{sample } i))^2 + (\text{depth}(\text{grid } j) - \text{depth}(\text{sample } i))^2}.$$

If there are no such samples, take the single spatially nearest sample’s membership. Call these memberships (each a number out of $1, \dots, K$):

$$z_1, z_2, \dots, z_{k'}.$$

where k' can be as low as 1, and as high as k . Then, predict the membership \hat{z} of the j th grid point by a majority vote of these memberships:

$$\hat{z}(\text{grid } j) = \text{mode}(z_1, \dots, z_{k'}),$$

and when there is a tie, choose the single nearest neighbor’s membership. Repeating this for each grid point $j = 1, \dots, B$, this process determines predicted province memberships $\hat{z}(\text{grid } 1), \dots, \hat{z}(\text{grid } B)$ for every grid point $j = 1, \dots, B$. (An example is shown in Step 2 and 3 of Figure 2.)

2.3 Assessing stability of newly learned provinces

Once an analyst has newly learned provinces on a given dataset, it is useful to quantify the associated uncertainty. In order to assess how *stable* an estimated province is, we devise a subsampling strategy for the dataset. Specifically, we randomly subsample 70% of the ASVs in a dataset, and calculate how often the predicted memberships on a grid persist across subsampling. This method proceeds in these four steps:

Step 1. For each compositional sample \mathbf{p}_i (for $i = 1, \dots, n$), resample 70% of the ASVs in \mathbf{p}_i and renormalize to sum to one, to obtain a shorter $\mathbf{p}_i^{(l)}$. Repeating this 100 times (for replicates $l = 1, \dots, 100$) to obtain 100 subsampled compositions $\{\mathbf{p}_i^{(l)}\}_{i=1, \dots, n, l=1, \dots, 100}$.

Step 2. For each new subsampled dataset $\{\mathbf{p}_i^{(l)}\}_{i=1, \dots, n}$, rerun `bioprovince` to obtain new province definitions at fine grid points $j = 1, \dots, B$.

Step 3. Re-align the K cluster labels in each of the results (so that a given cluster number k is consistent across all subsampled datasets), according to their geographical similarity.

Step 4. Then, for each grid point $j = 1, \dots, B$, assess the *stability* of the province as the frequency with which grid point j was deemed the most common province k_j , defined shortly.

We further describe some details. In order to realign the K clusters, we apply the Hungarian matching algorithm to the pairwise differences between the K clusters, where the pairwise difference between province $k_1 \neq k_2$ is measured as the average spatial distance between all samples in cluster k_1 and all samples in cluster k_2 . To measure the stability, we measure the relative frequency that grid point j is deemed cluster k_j , where k_j is the most frequent cluster:

$$k_j = \text{argmax}_{k=1, \dots, K} (\# \text{times gridpoint } j \text{ is deemed cluster } k),$$

and

$$\text{Stab}_j = \frac{\# \text{times gridpoint } j \text{ is deemed cluster } k_j}{100}.$$

Appendix Figure 11 and 12 shows an example of this, where grid points over latitude and depth are colored by the province membership k_j , and the opacity is proportional to Stab_j .

2.4 Choosing hyperparameters

In this section, we provide data-driven strategies for determining the hyperparameters for **bioprovince**. We recommend picking them in a particular order ($r \rightarrow \alpha \rightarrow K$) prior to applying the bioprovince algorithm.

1. Calculate a value r (relative importance of latitude versus depth)
2. Pick a value of α for clustering, using a visualization technique (described below).
3. For this α , pick number of clusters K , using within-sample variance.

The hyperparameter r governs the relative importance of latitude (in degrees) and depth (in meters) in our proposed pipeline. Since each cruises’ data covers widely different spatial ranges, the use of a single r parameter harmonizes the spatial scale of clustering among cruises. We devise a method resemblant of distance decay [38] from macroecology, which proceeds as follows. First take all pairs of samples’ (a) biological distances, (b) latitude difference, and (c) depth difference. Next, take only the sample pairs that are reasonably close to each other. Then, for sample pairs in each cruise, apply two separate linear regressions of (a) onto (b) and (c), and take the *weighted* average of the significant positive estimated slopes from each cruise – using the number of sample pairs as relative weights. The ratio of those averaged slopes determines r . The full procedure is described in Appendix section 2.

Next, in order to quantify α – the relative amount of biological and geographical information being used by clustering (in Step 1) – we develop a visualization strategy that allows the user to pick an appropriate value. First create four additional synthetic samples, whose spatial locations are at the four corners of the latitude-depth rectangle of the existing samples, and whose biological information are randomly drawn from samples in the existing dataset. Having compressed this augmented dataset into two dimensions using multidimensional scaling (MDS), take the proportion of points (out of n) that are contained within a polygon whose vertices are those four points. This is a randomized metric (between 0 and 1) that measures how *saturated* with spatial information the distance matrix D from (4) has become. We also form a “null” version of this metric (described in Appendix 3. In short, non-null scores use the four corners in space as an actual reference, while the null scores pick four random spatial points. Both the null and non-null metrics can be recalculated multiple times, where the replicates come from repeatedly picking four random values (from the data itself) of biological compositions for those four corners. The value α (between 0 and 1) should then be chosen to be a value where the null and non-null values are still highly overlapping.

Lastly, we describe how to determine a suitable number of clusters K . For each candidate value of $K = 1, 2, \dots$, conduct clustering (using **biocluster**), then calculate a within-cluster distance according to the mixture distance (4):

$$\text{Average within-cluster distance} = \sum_{k=1}^K \sum_{i_1 \neq i_2, i_1, i_2 \in C_k} D_\alpha[i_1, i_2],$$

for D_α defined in (4). Then, choose a suitable value of K visually, by identifying an “elbow” location where the improvement in the average within-cluster distance sharply diminishes as k increases. The first panel of Figure 2 shows an example applied on data from the P16S cruise.

Lastly, after the **biocluster** sample clustering is done with these chosen hyperparameters, we recommend choosing the value of k – for k -nearest-neighbor prediction – using visual inspection of the resulting province estimates. A small integer k between 1 and 5 is usually suitable and creates spatially coherent provinces; a larger k is useful when the estimated cluster memberships at the samples substantially overlap in space, and all clusters consist of a sufficiently large number of samples.

3 Results

3.1 Application to one cruise

We first applied our pipeline to a single cruise, P16N, from the GRUMP dataset. The three panels in Figure 2 show the result of applying each step of our **bioprovince** algorithm. Step 0 (top-left panel) shows the simulated scores (Appendix 2.4) – both null and non-null). We pick a value of $\alpha = 0.1$ for which there

is substantial overlap between these two scores’ distributions. Then, in the second part of Step 0 we use the within-cluster distance (Section 2.4) across candidate values of $K = 1, 2, \dots$, and in this case, we identify an elbow at $K = 7$.

Next, we determine how different pairs of samples should be by forming a pairwise distance matrix that is, entrywise, a convex combination of biological distance and spatial distance (using an α and $1 - \alpha$ mix). Then, we apply our clustering algorithm **biocluster** with these hyperparameters to estimate cluster memberships of the samples as shown in Step 2 (left bottom panel of Figure 2). Lastly, in Step 3, we perform **bioprovince** – a nearest-neighbor prediction of memberships – on a fine grid in latitude-depth and based on localized abiotic similarity, to define seven different biological provinces.

The resulting provinces capture strong spatial and vertical structure in the Pacific. Two well-defined oligotrophic clusters occupy subtropical surface waters, while higher-latitude and deeper waters are divided into several additional provinces. Each province forms a coherent, internally consistent community distinct from its neighbors, demonstrating that the algorithm delineates biologically meaningful domains along the transect without relying on predefined geographic boundaries or environmental thresholds. Having demonstrated the workflow on a single cruise (P16N), we next applied the **bioprovince** algorithm to a broader dataset of five Pacific Ocean cruises to examine biological structure across larger spatial and temporal scales.

3.2 Applying bioprovince algorithm across broad latitudinal transects in the Pacific from poles to the tropics

We structured the analysis in two main steps:

1. Pooled clustering across five cruises - We combined phytoplankton samples from all five cruises and applied the clustering algorithm to identify coherent communities across the full dataset. (See Section 3.2.1, Figure 3)
2. Defined 3-dimensional provinces (which we will call 3D-provinces) from the poles to the tropics - Using pairs of cruises along latitudinal transects, we estimated biological provinces to reveal how communities vary from the equatorial Pacific to high-latitude waters. (See Section 3.2.2, Figures 5, 6, 7.)

3.2.1 Biologically clustering five cruises’ pooled data

Here, we applied the **biocluster** algorithm to the pooled dataset from all five cruises, resulting in 16 distinct biological clusters or “biocluster” that are depicted within each cruise’s panel (Figure 3). Hereafter, we adopt the notation of [cruisename]-[cluster] to refer to a biocluster in a particular cruise’s panel, for notational brevity.

Our algorithm found that 10 out of the 16 bioclusters are symmetrically distributed across the equator, confirming the intuition that the biological compositions are likely to be similar in the same environmental conditions but mirrored at the same latitudinal locations across the equator. We found the biological clustering to be *robust* in the pooled dataset of multiple cruises. That is, even though the five cruises spanned highly variable dates, seasons, and spatial locations, nearby samples consistently clustered together and occupied similar spatial locations within the Longhurst provinces. (For a numerical comparison, see Appendix Table 8). For instance, the upper $\sim 100\text{m}$ of the oligotrophic gyres in either hemisphere (i.e., SPSG and NPTG) are predominantly associated with bioclusters 3 (e.g., P16S-03, P16N-03), 4 (e.g., P15S-04, P16N-04), 5 (e.g., G2-05, G3-05), and 6 (e.g., P16S-06, G2-06). At a coarse taxonomic resolution, the similarity among bioclusters 3 through 6 is primarily driven by the dominance of *Prochlorococcus* ($\sim 82 - 92\%$) along with co-occurrence of other picophytoplankton (e.g., *Synechococcus*, pelagophytes) and nanophytoplankton (e.g., prymnesiophytes, dictyochophytes) at much lower abundance (Figure 4).

Also, these oligotrophic gyres are separated by biocluster 1 in equatorial waters, indicating a persistent phytoplankton community within the upper $\sim 100\text{m}$ (e.g., P15S-01, P16N-01). While these communities share similar picocyanobacterial members with those in the oligotrophic gyres (i.e., *Prochlorococcus*: $\sim 83\%$), biocluster 1 also has an increased relative contribution from diatoms and pelagophytes (Figure 4). In deeper waters, we find another coherent biocluster 2 across multiple cruises (e.g., P15S-02, P16S-02, P16N-02) which is characterized by higher relative amounts of eukaryotic phytoplankton ($\sim 32\%$ with a standard deviation of $\sim 14\%$) including diatoms, prymnesiophytes, and pelagophytes (Figure 4). Additionally, it seems

Bioprovince algorithm workflow (demonstrated on P16N cruise)

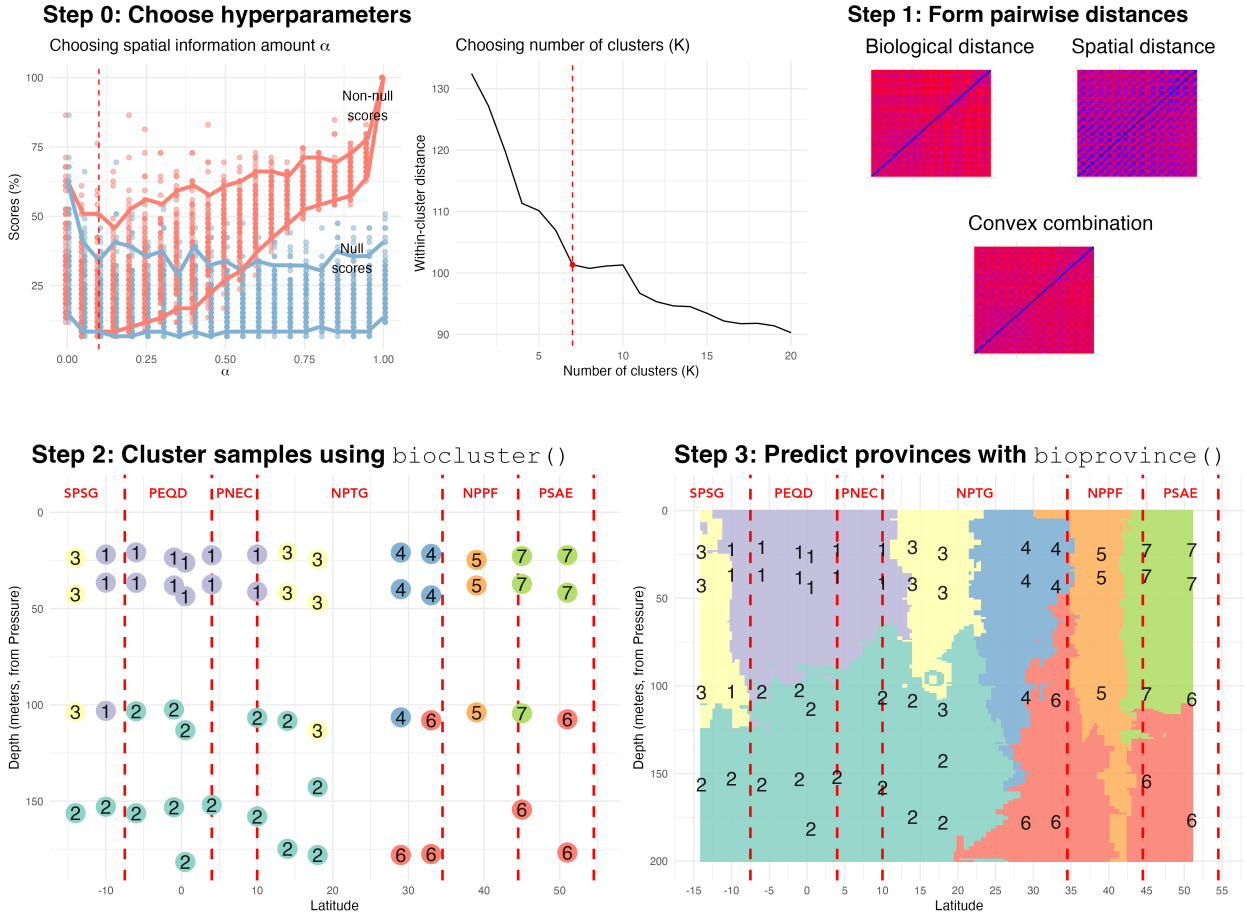


Figure 2: Applying the pipeline to a single cruise (P16N), as described in Section 2.2. The first panel describes the hyperparameter tuning described in Section 2.4. The second panel shows an example of forming a convex combination of distances between samples. The third panel shows the estimated clusters at the sample locations, shown as numbered points, obtained using the `biocluster` algorithm. The fourth, last panel shows the result of applying the `bioprovince` algorithm to conduct a localized nearest-neighbor 3D-province prediction on a fine spatial grid. The 3d-province predictions are shown in discrete colors.

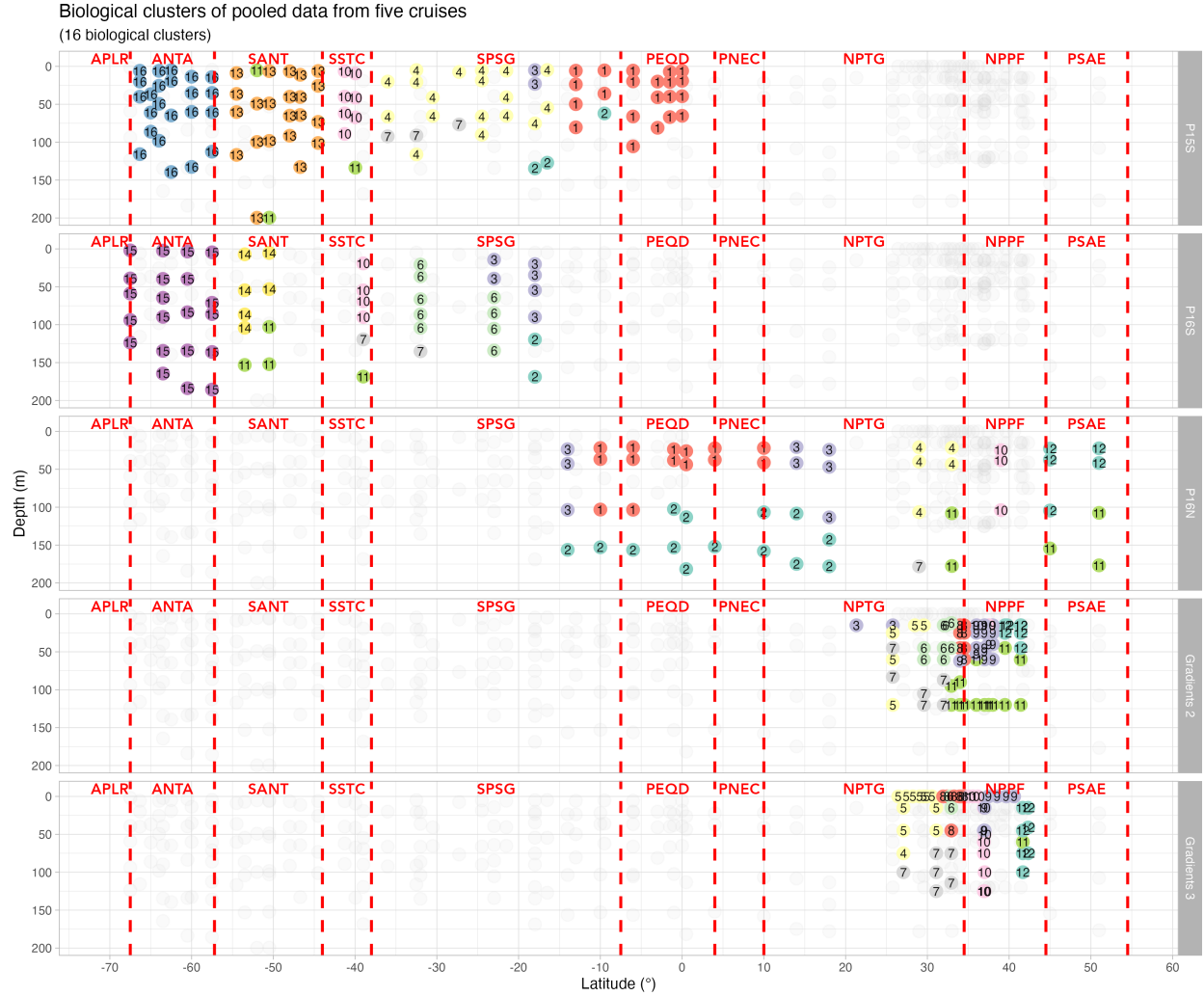


Figure 3: *Biological clusters of samples from the pooled dataset of five cruises (P15S, P16S, P16N, and Gradients 2 & 3), where each row shows the samples from one cruise at a time. The colors and numbers show the cluster memberships estimated at the sample location, and Longhurst boundaries are shown in vertical red lines.*

that frontal zones (e.g., S. Subtropical Convergence Province – SSTC, NPPF) – which separate oligotrophic gyres from subpolar regions – consist of the same biocluster (P15S-10, P16S-10, P16N-10) across three cruises. The phytoplankton composition of biocluster 10 (Figure 4) shows a mixed community structure consisting of relatively greater proportions of *Synechococcus* especially in the northern hemisphere ($\sim 51\%$ in Gradients cruises, and 11.9% in the P16S&N cruises) and eukaryotic phytoplankton ($\sim 45\%$ with a standard deviation of $\sim 16\%$) such as picoeukaryotes, nanophytoplankton, and diatoms (Figure 4). In the higher latitude waters poleward of these frontal regions, there is a pronounced increase in eukaryotic phytoplankton abundance for bioclusters 11 - 16 ranging from about 14% to 100% (Figure 4).

3.2.2 Analyzing 3-dimensional biological provinces

Here we detail 3D-provinces derived by applying `bioprovince` to pooled datasets of two cruises at a time: P16S with P16N, and Gradients 2 with Gradients 3. This pairing was specifically chosen because the data for each pair were collected during the same time of year. The pooled P16S and P16N dataset represents a sparsely sampled, but geographically extensive, north-south Pacific Ocean transect. In contrast, the pooled

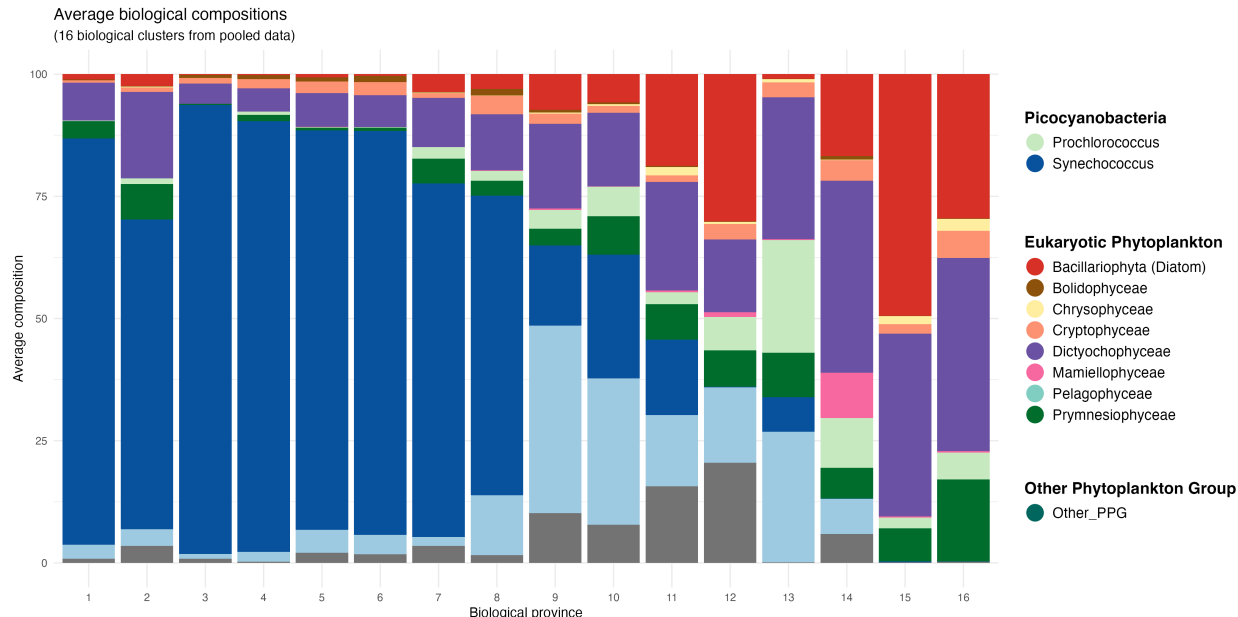


Figure 4: (Left panel) The average relative composition for each of the 16 biological clusters from the pooled samples from five cruises, aggregated at the ecologically relevant plankton group level, and visualized as barplots. The clusters have been ordered in ascending order of the average distance away from the equator.

Gradients 2 and Gradients 3 dataset provides a dense sampling of a more geographically compact area. These two distinct datasets offer a valuable opportunity to evaluate the respective merits and drawbacks of wide-scale, sparse sampling versus localized, dense sampling for the delineation of biological provinces.

We can see in Figure 5 (Panel A1, A2) that our 3D-provinces line up well with existing Longhurst boundaries, while additionally revealing much finer spatial partitions across latitude and depth. Figure 6 summarizes the results using 2-way cross-tabulated tables across the two categories: (1) 3D-provinces as columns, and (2) Longhurst provinces as rows. Each row’s measurements show that some Longhurst province match exactly with our novel 3D-province (e.g., ANTA which matches 3D-province 9 100% from the paired P16S/P16N cruise) (Figure 6).

In the oligotrophic gyres, which are classically divided into only two Longhurst provinces (SPSG and NPTG), our **bioprovince** algorithm finds much more biologically distinct 3D-provinces. For example, Longhurst province SPSG is subdivided into three 3D-provinces 3, 4, and 5 (23.1%, 23.1% and 34.6% respectively) in the upper euphotic zone, and 2 and 8 (15.4% and 3.8%) in the deeper euphotic zone. Similarly, Longhurst province NPTG consists of 3D-provinces 3, 4, and 5 (11.8%, 17.6% and 29.4%) in the upper euphotic zone, and 2 and 8 (23.5% and 17.6%) in the deeper euphotic zone. Our results also identify the upper euphotic zone of the equatorial Pacific (3D-province 1) as an important ecological boundary separating the oligotrophic regions of the N and S Pacific (Figure 5 panels A1 and B1). Interestingly, the classical Longhurst province PEQD does not specify depth-wise separation in equatorial waters, while our 3D-provinces clearly split this region into two – one upper layer (3D-province 1, 53.3%) and one deeper layer (3D-province 2, 46.7%). Moving poleward from oligotrophic gyres, our algorithm identified transitional 3D-provinces (6 and 7) separating those gyres in the upper 100 meters from higher-latitude 3D-provinces (9–11). These higher-latitude provinces exhibited greater taxonomic variability and relative abundance of eukaryotic phytoplankton (Panel B of Figure 5).

Finally, in Figure 7 we overlay the biological and Longhurst classifications on the abiotic conditions at the samples from the two cruises P16S & P16N. We first see from Panel A that the samples are impossible to properly cluster with temperature and salinity alone, as no natural groups emerge that are distinguishable from others. Longhurst provinces explain away some of the variation in temperature and salinity – as shown in Panel B. However, the biological clusters (shown as numbers) partition the samples much further than the Longhurst provinces (shown as shapes). Furthermore, Figure 7 Panel C show the 3D-provinces in

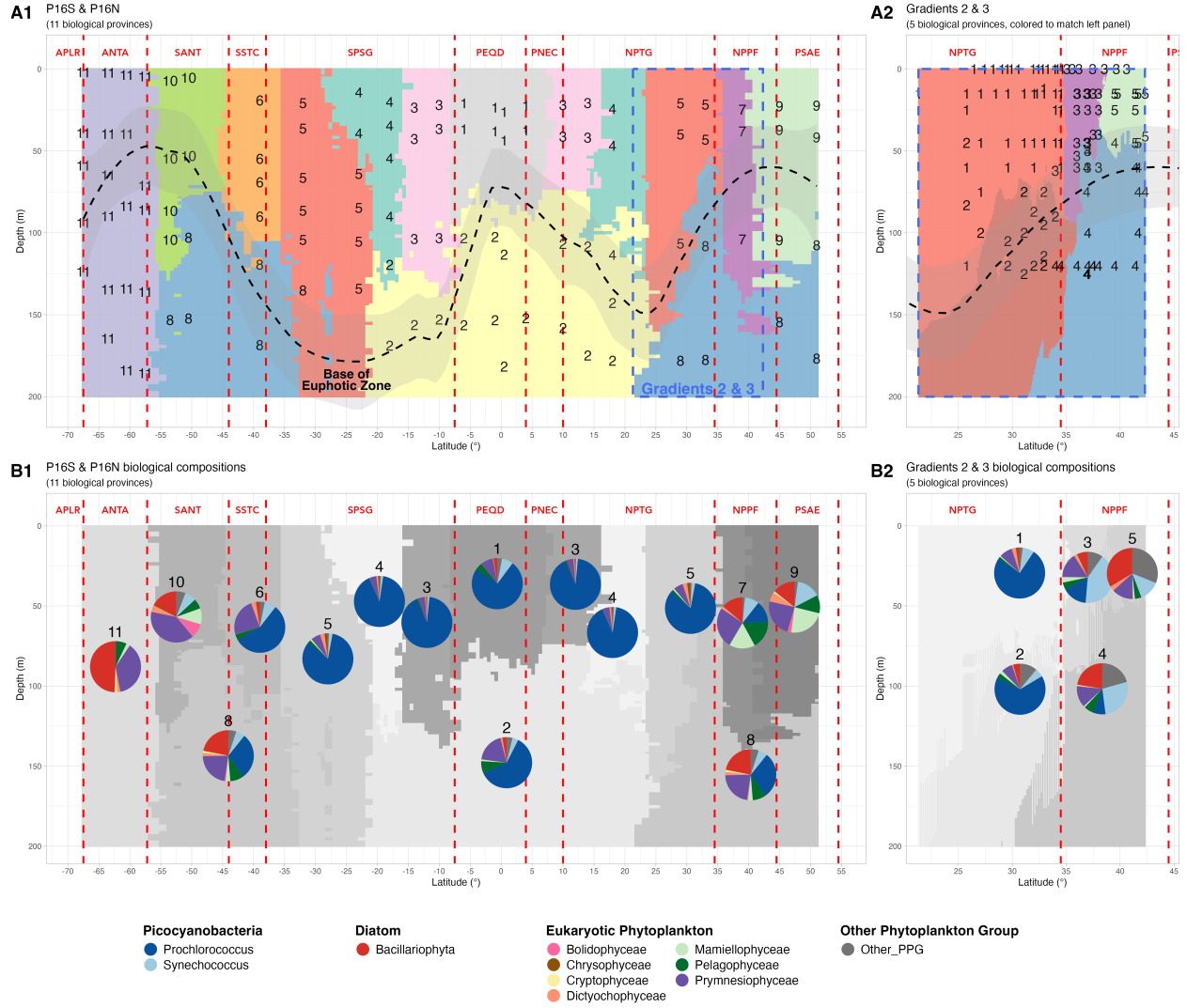


Figure 5: Comparing the estimated provinces from applying bioprovince to two cruises at a time (P15S & P16N, and Gradients 2 & 3). [Top row] Colors show the estimated province, and the numbers show the cluster memberships estimated at the sample locations. Longhurst boundaries are shown in vertical red lines, and three oceanographic fronts are shown in grey boxes. Also, the dashed black line shows the estimated base of the Euphotic Zone, calculated from the Darwin simulation model as the depth at which the sunlight (PAR) is 1% of the surface level. The shaded black ribbon region shows the standard error for this dashed line. [Bottom row] The average relative composition for each bioprovince, at the ecologically relevant plankton group level, is shown overlaid over greyscale background in which each province is now shown as a greyscale shade. Barplots of average compositions can be found in Appendix Figure 9.

Comparison of novel 3D provinces to Longhurst
(Normalized so that rows sum to 100%)

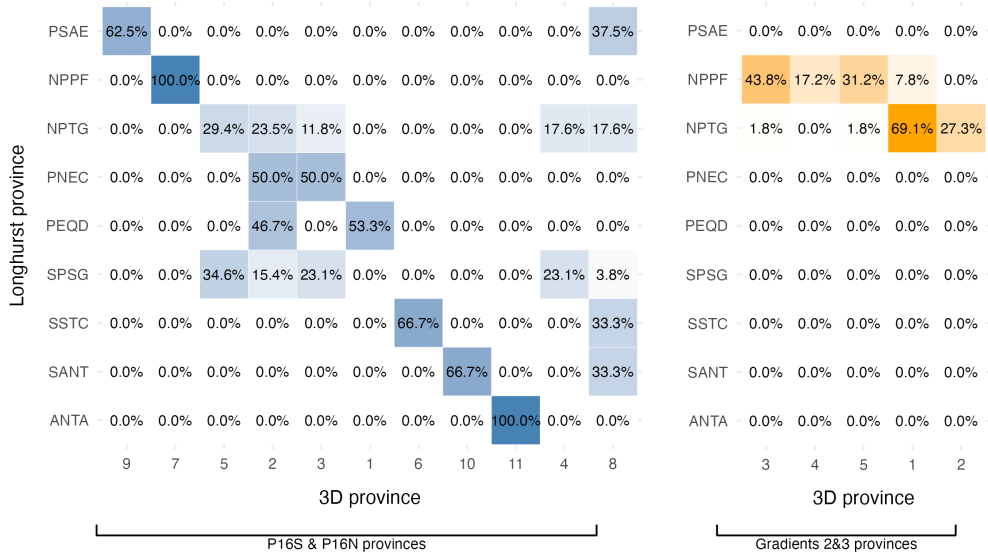


Figure 6: Comparison of novel biological provinces to Longhurst provinces, in a normalized cross-tabulated table. Colors in each cell show the percentage. Rows (Longhurst provinces) are arranged from north to south, and each row’s entries have been normalized to 1. The provinces have also been arranged from left to right according to the most highly corresponding province to each Longhurst province. The left panel shows the biological provinces from the pooled P16S & P16N data, and the right panel shows the biological provinces estimated from the pooled Gradients cruise data.

temperature-salinity dimensions, and Panel D shows it on the principal components’ space of seven abiotic factors. In both plots, it is clear that (1) the abiotic conditions of the ocean alone are not adequate for finding biological clusters, and (2) the novel genomic metabarcoding data we are using is highly useful for defining new biological clusters and provinces.

4 Discussion

4.1 Insights from a single-cruise application

Our biological clusters and 3D-province estimates from the P16N cruise data (Figure 2) are consistent with studies of the same region that leveraged biogeochemical measurements to identify major differences in primary productivity across several known Longhurst provinces boundaries [39]. Specifically, the algorithm reproduces the separation between oligotrophic gyres—such as the South Pacific Subtropical Gyre (SPSG) and North Pacific Tropical Gyre (NPTG)—and regions of elevated productivity, including (i) equatorial waters in the North Pacific Equatorial Countercurrent (PNEC) and Pacific Equatorial Divergence (PEQD) provinces, (ii) frontal regions like the North Pacific Polar Front (NPPF), and (iii) subpolar regions such as the Pacific Subarctic Gyres Province (East) (PSAE) (Figure 2). Beyond confirming these known patterns, the **bioprovince** approach reveals previously uncharacterized microbial community structure at depth, highlighting coherent vertical organization within each Longhurst province that is largely invisible in surface-only analyses (Figure 2). This deeper structure underscores the value of integrating high-resolution ASV data, demonstrating that biologically meaningful provinces extend beyond latitudinal productivity gradients and into the three-dimensional structure of the water column.

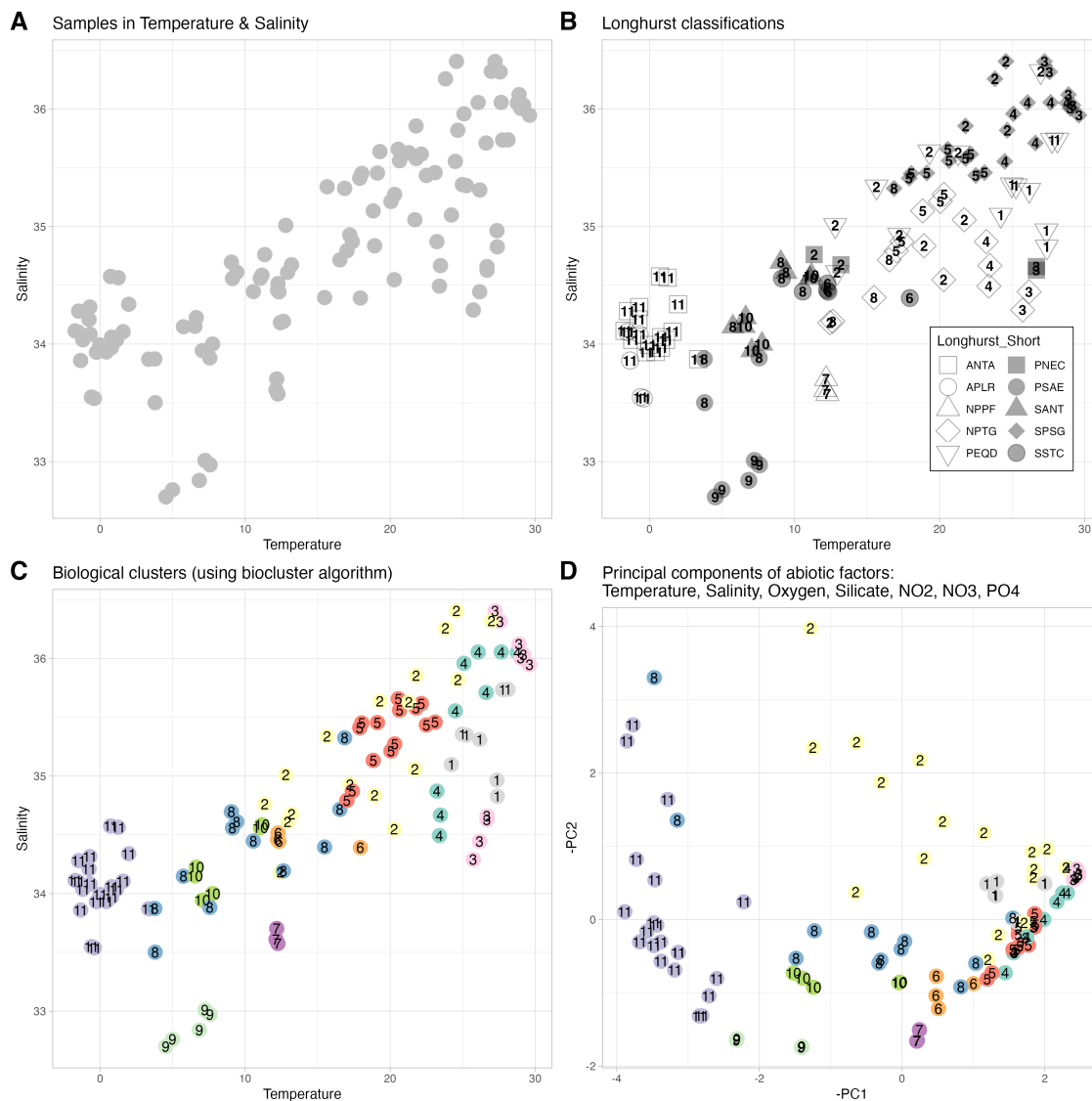


Figure 7: (Left panel) The 11 clusters from P16S & P16N samples in temperature-salinity space; the points are slightly jittered to show all overlapping points. (Right panel) The same 11 clusters of samples in the Principal Components space of five abiotic factors (Temperature, Salinity, Oxygen, Silicate, NO₂, NO₃, PO₄).

4.2 Oceanographic drivers of phytoplankton community structure

We extend the application of the **bioprovince** framework by pooling together five latitudinal cruises in the Pacific Ocean from the GRUMP dataset. The analysis revealed 16 distinct biological clusters that capture both surface and depth-resolved variation in phytoplankton communities (Figure 3). These findings support the coupling between physical, chemical, and biological processes that organize marine phytoplankton communities. For instance, continuous wind-driven upwelling in the equatorial Pacific enhances nutrient supply, supporting elevated new production in these high-nutrient, low-chlorophyll waters [40, 41]. In this region, we observe the recurring presence of biocluster 1 (i.e., P15S-01, P16N-01) across multiple cruises (Figure 3). Beneath the upper euphotic zone, another distinct biocluster (e.g., P16N-02) emerges, characterized by higher relative abundances of eukaryotic phytoplankton such as diatoms, prymnesiophytes, and pelagophytes, consistent with enhanced nutrient availability in the equatorial Pacific waters that separate two major oligotrophic gyres (Figure 4).

Poleward from the oligotrophic gyres, the decline of *Prochlorococcus* and the rise of larger phytoplankton taxa, such as diatoms and bolidophytes, also coincide with increasing nutrient availability, marking additional transitions across environmental gradients that similarly support higher primary productivity [28]. Beyond shifts in environmental gradients, this collapse with the *Prochlorococcus* populations has also been shown to be impacted by ecological interactions (e.g., shared predation, impact of viruses) [42, 43]. Remarkably, the patterns of these bioclusters appear symmetrical across hemispheres and also extend into deeper waters (Figure 3). This suggests that at equivalent latitudes relative to the equator, similar bioclusters—and by extension, comparable ecological niches—occur in both the northern and southern Pacific. These observations further prove that the GRUMP dataset is highly consistent and comparable across different data collection methods in the same spatial latitude-depth area.

Seasonal variability further influences biocluster assignments. For example, samples collected across comparable latitudes in the P15S and P16S cruises exhibit different biocluster memberships in similar Longhurst regions. Similarly, in the N. Pacific (i.e., NPTG, NPPF, PSAE) samples collected in the same region across three separate cruises (P16N-12, G2-12, G3-12) all belong to biocluster 12, but with P16N-12 located significantly more poleward than G2-12 and G3-12 – highlighting seasonally *shifting* ecological niches within the NPTZ. In sum, we see in our analysis that when data collected in very different seasons are pooled together, the samples’ estimated clusterings are often due not to purely spatial difference, but due to the seasonality difference. The two are hard to disentangle and without significant postprocessing to post-hoc combine certain biocluster memberships, it is challenging to use the bioprovince algorithm for geographically coherent and interpretable 3D-provinces. Thus, we recommend defining 3D-provinces only from data pooled from cruises taken at a similar time of year. In Section 3.2.2, we do precisely this and discuss the results in the following section.

4.3 Ecological insights from 3-dimensional provinces

By combining data across paired cruises sampled during similar times of the year, the **bioprovince** algorithm resolves biologically coherent 3D-provinces that extend the classic two-dimensional view of ocean biogeography. For example, within the oligotrophic gyres, since both the oligotrophic NPTG and ultra-oligotrophic SPSG exhibit very low chlorophyll-*a* concentrations with very high abundances of *Prochlorococcus* [16, 44, 45], the Longhurst framework delineates only two broad provinces. However, our method identifies multiple, vertically distinct 3D-provinces corresponding to unique ecological niches (Figure 5). This finer-scale partitioning is largely due to the granular, ASV-resolution survey of plankton in the GRUMP dataset which captures well-known niche differentiation among *Prochlorococcus* ecotypes. This includes: (i) high-light-adapted clades dominating the upper euphotic zone, while low-light-adapted ecotypes prevail at depth and (ii) a latitudinal transition from HLII to HLI ecotypes moving poleward towards cooler waters from the warmer, central oligotrophic gyres (Supp. Figure 14). This separation of *Prochlorococcus* ecotypes by light and temperature regimes has been well established using empirical observations in other ocean basins and laboratory-based culture studies [46, 47].

The deeper 3D-province boundaries (in Figure 5) are largely congruent with the base of the euphotic zone, which further demonstrates the controlling role of abiotic factors such as light availability in structuring phytoplankton communities (Figure 5 A1). One notable exception is the absence of a deep provincial boundary in the Antarctic region, suggesting greater homogeneity in phytoplankton distribution throughout

the water column that is likely driven by rapid particle sinking and strong vertical mixing [48, 49]. This vertical homogeneity in phytoplankton community structure, dominated by diatoms and prymensiophytes (Figure 5 B1), also illuminates the potential sensitivity of 3D-province boundaries to taxonomic scope. For instance, the inclusion of mixotrophic taxa such as dinoflagellates could reveal additional vertical transitions, as these organisms can persist across light and nutrient gradients by switching trophic strategies [50]. Overall, the 3D-provinces derived here highlight how integrating biological and environmental information can reveal complex ecological zonation in the ocean interior.

4.4 Comparison with conventional biogeographical frameworks

Our 3D-provinces exhibit strong concordance with established frameworks such as the Longhurst provinces, while simultaneously capturing finer vertical and latitudinal variation. Cross-tabulation analyses confirm that conventional Longhurst provinces are largely embedded within the new **bioprovinces** (Figure 6), underscoring that physical and chemical properties continue to structure large-scale marine biogeography. Notably, the near one-to-one correspondence between the Antarctic Longhurst province (ANTA) and 3D-province 11, as well as between two polar Longhurst provinces (PSAE and SANT) with 3D-bioprovince 9 and 10 in shallow waters, highlights that fundamental ecological boundaries are preserved even when defined via genomic data.

Going beyond simply validating the classical province framework, the **bioprovince** approach further reveals biologically meaningful refinements. In the North Pacific Transition Zone, the boundaries inferred from Gradients 2 and 3 data are displaced southward relative to the canonical NPTG/NPPF/PSAE divisions, likely reflecting seasonal shifts in frontal positions. We can further examine similar oceanographic features in the S. Pacific – specifically the Polar Front (PF), subtropical front (STF), and equatorial upwelling (EQ). These dynamic regions are well-studied by [9] (based on analyzing the densely sampled P15S cruise) as persistent *ecological* boundaries. Indeed, in our cruise-by-cruise data analysis (in Appendix Figure 10), novel 3D-province boundaries successfully separate distinct phytoplankton communities across all three regions (PF, STF, and EQ). This successful delineation is evident not only in the P15S cruise but also in the P16S and P16N cruises, which sampled the region approximately a decade earlier. By revealing 3D-province boundaries that persist across datasets collected across a long time period, our method corroborates findings in [9] regarding the importance of persistent oceanographic features as ecological boundaries.

Our methodology successfully utilizes deeper water abiotic conditions to extend the conventionally known province definition beyond surface-level delineation by revealing new coherent biological niches of deeper-water marine microbes – especially in the oligotrophic and equatorial waters. Additionally, it is clear the abiotic conditions alone would not allow for groupings made using biological conditions, as depicted in Figure 7. Collectively, these observations demonstrate that the **bioprovince** framework reconciles biological variability with physical and chemical oceanographic structure. By providing a data-driven, vertically resolved, and temporally robust view of marine ecological patterns, this approach complements and extends conventional frameworks, enabling a more comprehensive understanding of the factors shaping marine biodiversity across space and depth.

5 Conclusion

The ability to define biologically coherent 3D-provinces has important implications for ocean ecology and climate science. Our **bioprovince** algorithm provides a reproducible and objective means to partition the ocean into ecologically meaningful regions, which can improve the resolution and accuracy of biogeochemical and ecosystem models. By incorporating biological information directly, **bioprovince** enhances our understanding of how productivity, nutrient cycling, and microbial community structure vary through space and depth.

To further enhance the utility of this framework, a crucial next step is to develop a statistical model for microbial ASV compositions observed across both time and space that enables principled statistical inference of estimated cluster memberships. This model should explicitly account for the annual seasonal cycle of the ocean, which our **biocluster** analysis revealed to be one of the main drivers of community composition. Properly handling this temporal dependence in a statistical model will also allow for more robust out-of-sample province predictions in spatial locations farther away from existing samples, and in different times

of the year. In addition, such a statistical model may also include a regression component to explicitly use environmental factors (e.g., temperature, salinity, nutrients), which could further enhance its prediction ability at new locations.

Beyond phytoplankton, this framework can be readily extended to other microbial groups within the GRUMP dataset or applied to independent datasets such as the Atlantic Meridional Transect (AMT), bioGEOTRACES, or TARA Oceans. Temporal comparisons across historical and modern metabarcoding datasets could further illuminate how marine provinces shift seasonally or in response to climate variability. The **bioprovince** algorithm thus offers a generalizable approach for investigating spatial and temporal evolution in marine microbial biogeography, providing a foundation for integrating molecular observations into global oceanographic research.

Acknowledgments

This work was supported through grants by the Simons Collaboration on Computational Biogeochemical Modeling of Marine Ecosystems/CBIOMES (Grant ID: 1195553 to S.H.). This work was also supported by the Simons Foundation (CBIOMES-549943 to J.A.F.) and the National Science Foundation (NSF-OCE-1737409 to J.A.F.).

Data Accessibility

The GRUMP data is available at Simons CMAP (<https://simonscmap.com/catalog/datasets/GRUMP>).

Author Contributions

Rafael Catoia and Sangwon Hyun designed the analytical pipeline, performed numerical experiments, and wrote the statistical software accompanying this manuscript. Nathan Williams bioinformatically prepared ASV data and also provided contextual information assisting with the use of this data. Yubin Raut assisted with generating the ASV data, provided feedback on the statistical framework and its applications to the ASV data, and contributed to data interpretation. Jed Fuhrman supervised the data curation and advised the ecological interpretation. All authors contributed substantially to writing the paper.

1 Supplement: Additional figures

Additional figures (Figure 8 and 9) are shown here.

| Cluster | Proportion of samples from each cruise | | | | |
|---------|--|-------------|--------|-------|--------|
| | Gradients 2 | Gradients 3 | P15S | P16N | P16S |
| 8 | 7.7% | 38.5% | 26.9% | 11.5% | 15.4% |
| 9 | 33.3% | 33.3% | 16.7% | 5.6% | 11.1% |
| 7 | 53.6% | 3.6% | 10.7% | 17.9% | 14.3% |
| 3 | 11.1% | 0.0% | 11.1% | 44.4% | 33.3% |
| 13 | 36.8% | 36.8% | 0.0% | 26.3% | 0.0% |
| 11 | 42.1% | 10.5% | 0.0% | 0.0% | 47.4% |
| 1 | 0.0% | 0.0% | 15.8% | 73.7% | 10.5% |
| 16 | 50.0% | 50.0% | 0.0% | 0.0% | 0.0% |
| 2 | 0.0% | 4.2% | 75.0% | 20.8% | 0.0% |
| 4 | 0.0% | 0.0% | 60.0% | 40.0% | 0.0% |
| 15 | 68.2% | 31.8% | 0.0% | 0.0% | 0.0% |
| 14 | 31.2% | 68.8% | 0.0% | 0.0% | 0.0% |
| 5 | 0.0% | 0.0% | 100.0% | 0.0% | 0.0% |
| 6 | 0.0% | 0.0% | 100.0% | 0.0% | 0.0% |
| 10 | 0.0% | 0.0% | 0.0% | 0.0% | 100.0% |
| 12 | 0.0% | 0.0% | 0.0% | 0.0% | 100.0% |

Figure 8: *The mix of clusters from each cruise in the 16-cluster analysis of Figure 3 in Section 3.2.1. The table is sorted from top to bottom in order of how highly homogenous (mixed) those clusters' samples are across the five cruises. The homogeneity is measured using a KL divergence against an equal mix of five cruises. Here, 12 out of the 16 clusters are found are from multiple cruises – that is, those clusters consist of at least a 70%-30% mix (of samples) from two cruises. Only clusters 13, 14, 15, and 16 (all in Longhurst SANT and ANTA) originate entirely from a single cruise.*

2 Supplement: Full procedure for choosing r

We took all pairs of distances between the $n^{(l)}$ samples in the data for a single cruise (l) that are close enough to be relevant. (In our analysis, we isolate our attention to latitudes that are within 3 degrees, and depths that are within 10 meters.) Then we conducted a linear regression of (1) the difference in Aitchison distance onto (2) the latitude (degrees). Call this regression model: $d_{\text{bio}} = b_{01}^{(l)} + b_1^{(l)} \cdot d_{\text{lat}}$. The slope b_1 quantifies the degree of *decay* in biological similarity (as measured by Aitchison distance) as one moves away in latitude. Next, we conduct another linear regression of (1) the difference in Aitchison distance onto (2) depth (in meters). Call this regression: $d_{\text{bio}} = b_{02}^{(l)} + b_2^{(l)} \cdot d_{\text{depth}}$. Call $b_1 = \frac{\sum_{l=1}^5 b_1^{(l)} n^{(l)}}{\sum_{l=1}^5 n^{(l)}}$ the weighted average of the regression slopes of latitude; likewise, call $b_2 = \frac{\sum_{l=1}^5 b_2^{(l)} n^{(l)}}{\sum_{l=1}^5 n^{(l)}}$ the weighted average of regression slopes of depth.

In order to create a new rescaled version of latitude (call this `scaled_lat`) which has the same footing as d_{depth} , we multiplied latitude by a factor of $r = b_1/b_2$ to obtain the scaled latitude:

$$\text{scaled_lat} = \text{lat} \cdot \frac{b_1}{b_2}, \quad (5)$$

or equivalently, $\text{lat} = \text{scaled_lat} \cdot \frac{b_2}{b_1}$. Lastly, we see how $r = b_1/b_2$ should come into play in the spatial

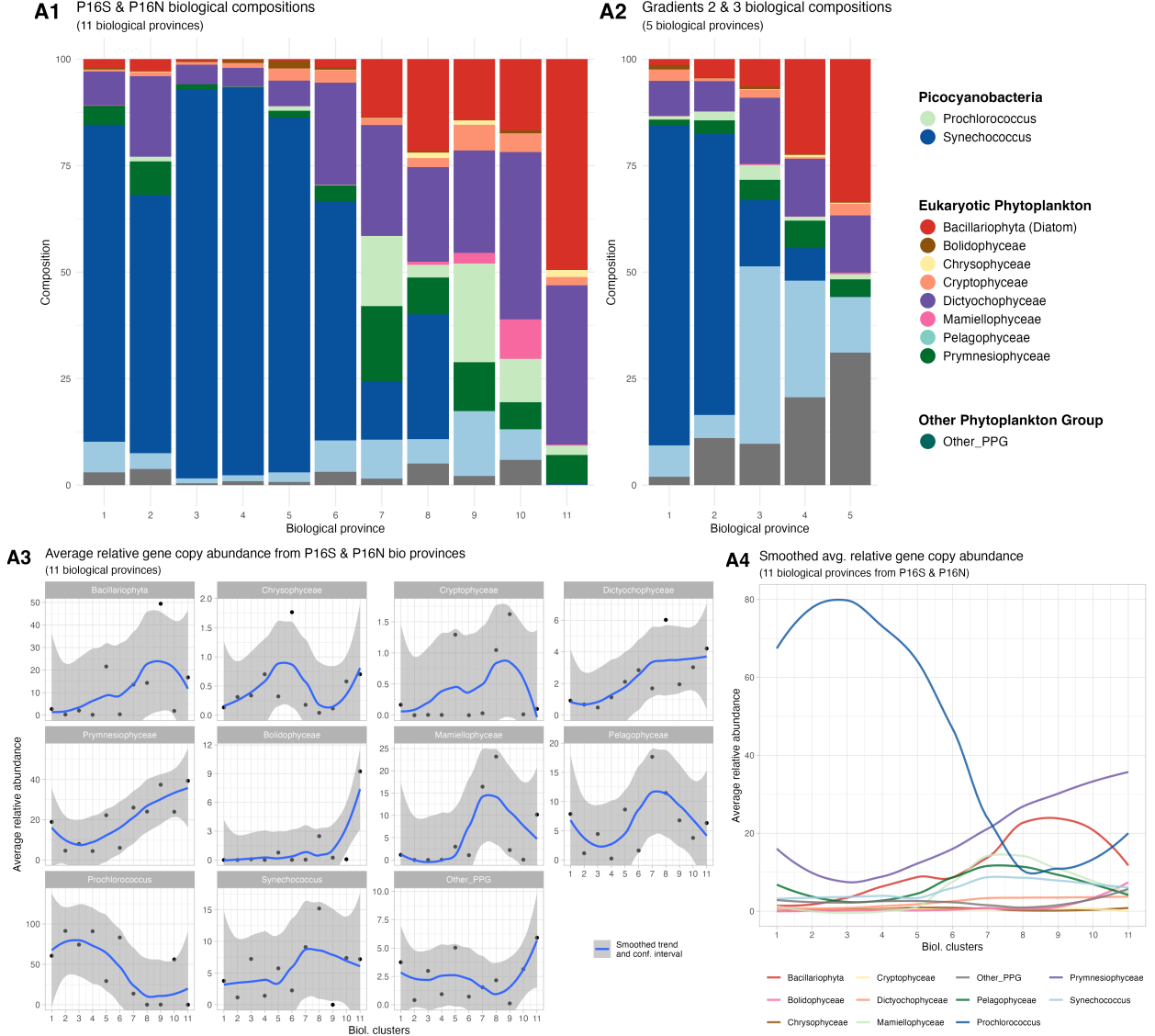


Figure 9: The average relative composition for each bioprovince, at the ecologically relevant plankton group level, is shown as barplots (top row) and line plots (bottom). This figure is supplementary to Figure 5.

distance between, say, two samples i_1 and i_2 :

$$\sqrt{(r \cdot \text{lat}(i_1) - r \cdot \text{lat}(i_2))^2 + (\text{depth}(i_1) - \text{depth}(i_2))^2},$$

which *upweights* latitude by a factor of r , plays the role of rescaling latitude to be equivalent to depth.

Figure 13 shows an example of the two types of regressions on each cruise. Here, the red slopes of the regression of d_{bio} onto scaled.lat in the right panel are similar in scale to the slopes of the regression lines of d_{bio} onto depth in the left panel. This visually verifies that the rescaling of latitude results in a similar rate of decay in biological similarity over both rescaled latitude and depth.

3 Supplement: Full procedure for choosing α

First, augment the compositional dataset P with four rows that are randomly selected four compositions from the existing dataset P . Then, form a scaled $(n + 4) \times (n + 4)$ pairwise Aitchison distance matrix $D_{\text{bio}}^{\text{aug}}$

Province predictions in Pacific ocean using bioprovince algorithm

Separate application on 5 north-south transect cruises (over 9 Longhurst regions)

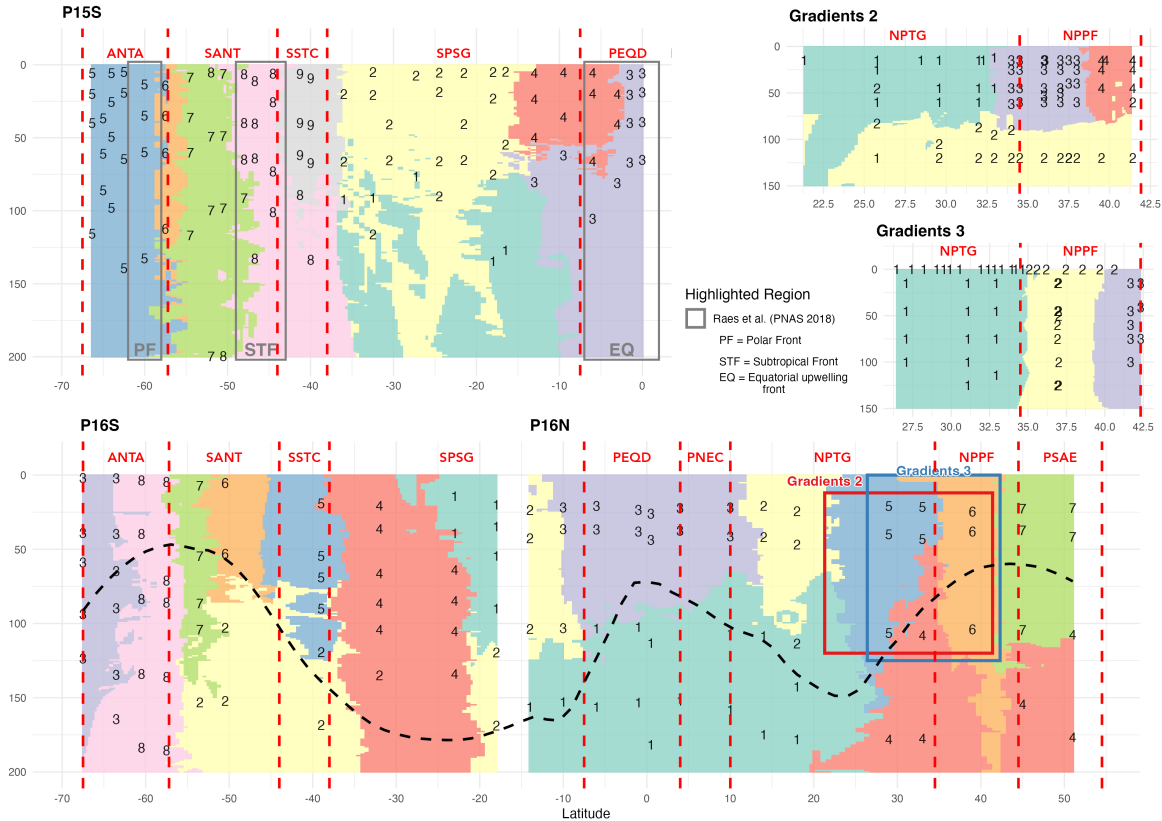


Figure 10: Comparing the estimated provinces computed separately from the five transect cruises. Colors show the estimated bio-province, and the numbers show the cluster memberships estimated at the sample locations. Longhurst boundaries are shown in vertical red lines. The top-left figure (P15S) also shows bio-diversity fronts from [9]. The bioprovince estimates in Figure 2 and the current Figure 10 are consistent with several well-established boundaries between Longhurst provinces that separate oligotrophic gyres (e.g., SPSG, NPTG) from regions of elevated primary productivity, including equatorial waters (e.g., PEQD, PNEC), frontal zones (e.g., NPPF, SSTC), and subpolar and polar regions (e.g., PSAE, SANT, ANTA).

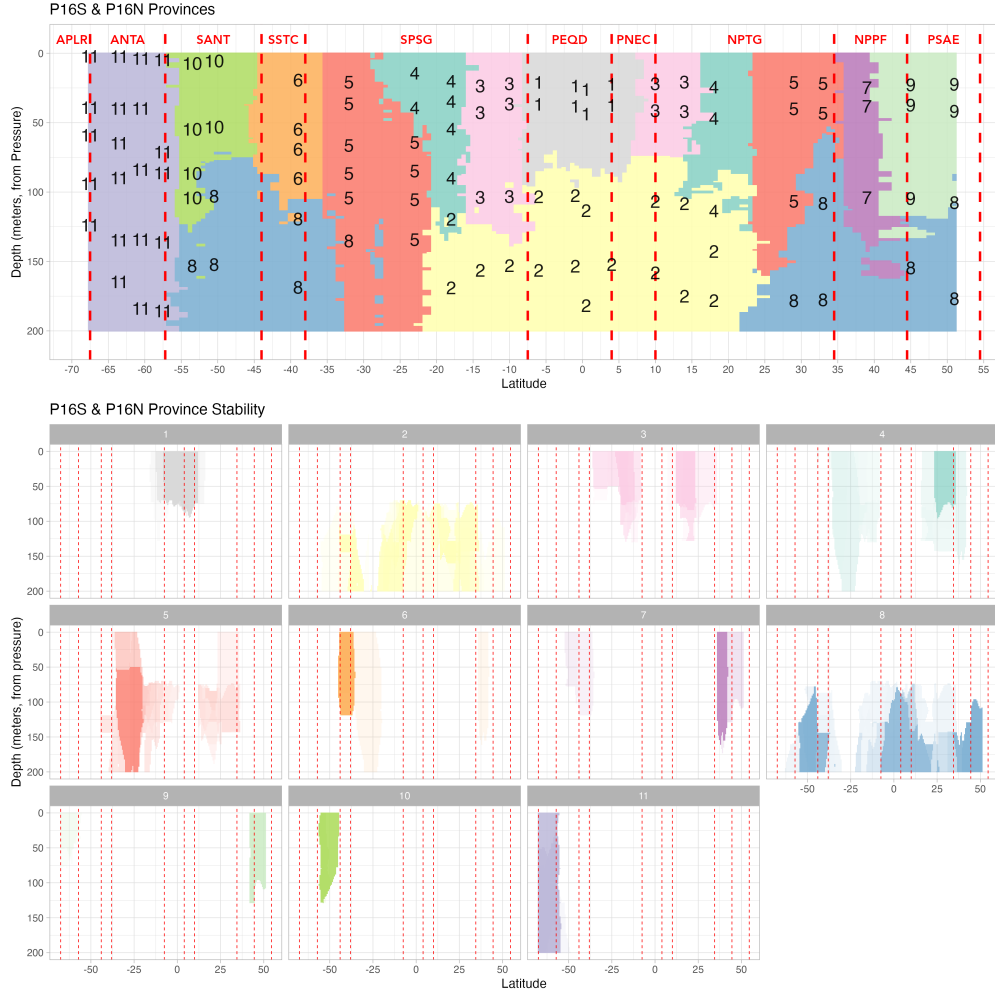


Figure 11: *Plotting the stability 2.3 of province estimates for P16 cruise data. The top panel reproduces the provinces estimated from data from the pair for cruises (P16S and P16N), and the bottom plot shows the stability estimates of each 3d-bioprovence in separate panels, with opacity of the color proportional to the stability. Notably, the surface provinces appear more stable, while the two deeper provinces are less stable, especially with respect to the province estimates in the top panel.*

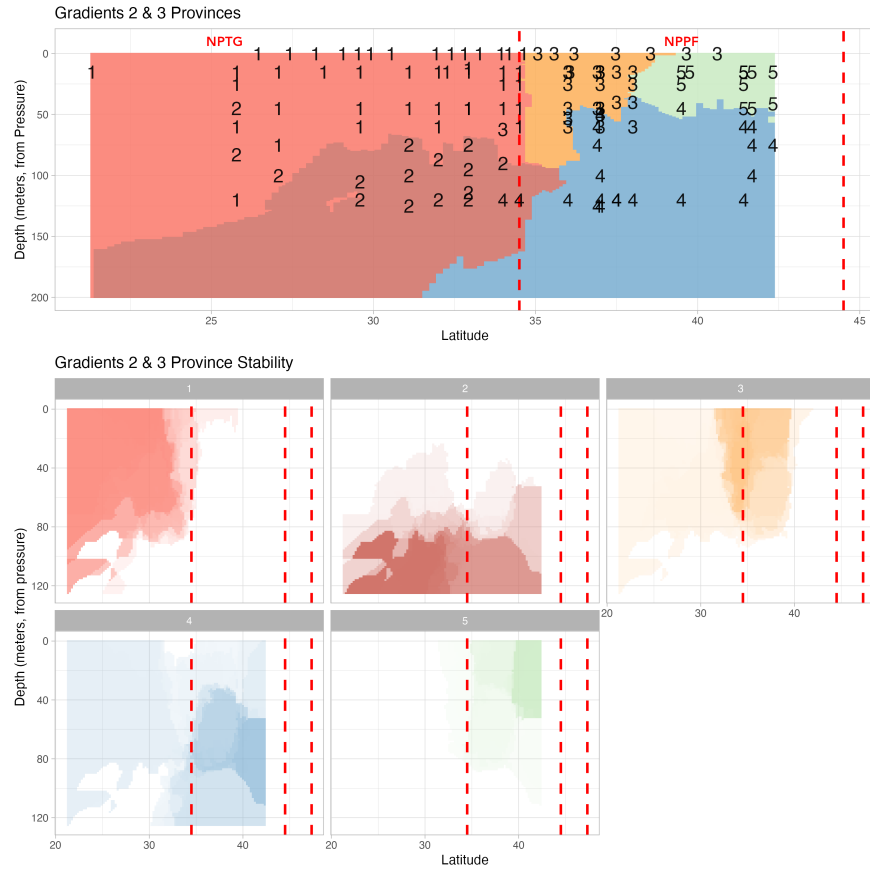


Figure 12: *Plotting the stability of the province predictions 2.3 for Gradients cruise data. The top panel reproduces the provinces estimated from data from the pair of cruises Gradients 2 & 3, and the bottom plot shows the stability estimates of the province predictions in separate panels, with opacity of the color proportional to the stability.*

Choosing r (for rescaling latitude)

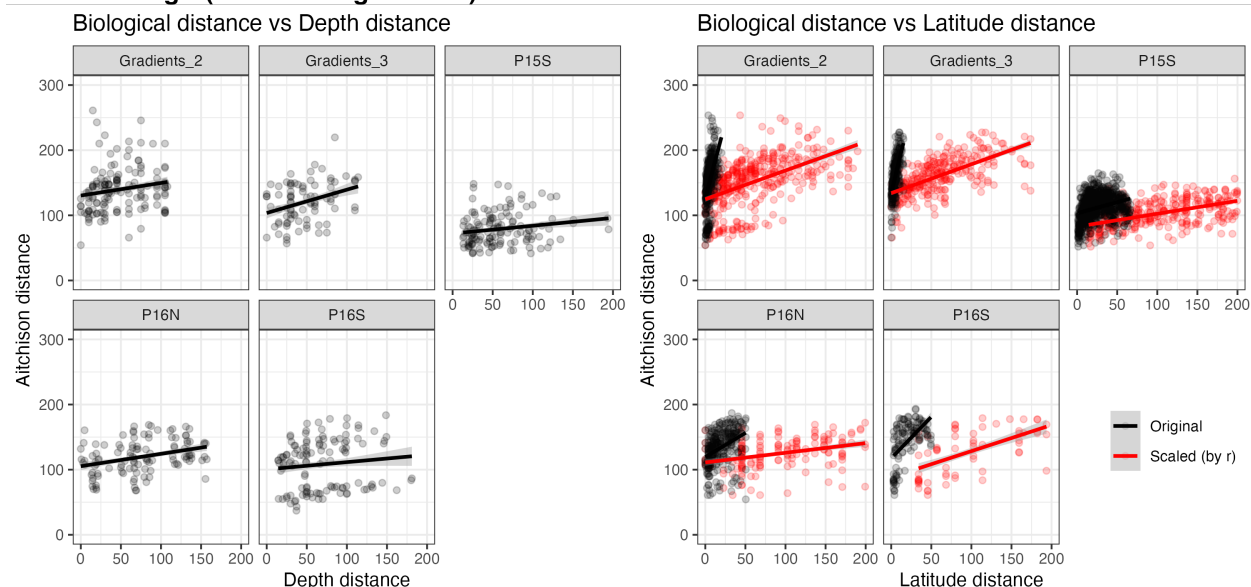


Figure 13: The left panel shows a scatterplot of the pairwise biological distances (measured by Aitchison distance of the compositions at each pair of samples) between samples (y axis) over the depth distance between samples (x axis) using black points, as well as a linear regression line. Each subpanel shows this analysis from one cruise. The slope of the regression approximately measures the speed of decay in the biological similarity as one moves farther away in depth. Next, the right-hand-side shows a scatterplot of the biological distances and the latitude distance in black points, with a linear regression line. The red points, show the scaled distances scaled_lat from (5) as x values instead, and the corresponding linear regression of biological distances on scaled_lat. The red slopes are comparable in size to the left panel's slopes, which verifies visually that the rescaling of latitude is sensible.

of the augmented $(n+4)$ compositions as in (1). Also augment the latitude and longitude by four points that are placed at the four corners in latitude and depth. Then, calculate the scaled $(n+4) \times (n+4)$ distance matrix as in (3), $D_{\text{spatial}}^{\text{aug}}$. After scaling both $D_{\text{bio}}^{\text{aug}}$ and $D_{\text{spatial}}^{\text{aug}}$, take an entry-wise convex combination as in (4) to form D^{aug} . Next, using this matrix, form a 2-dimensional multidimensional scaling (MDS) plot, and count the relative number of the points in the MDS coordinate space that are in the *convex hull* connecting those four points.

Repeat this $L = 100$ times to calculate this score $n_l(\alpha)$ for the l 'th replicate. Also call the *null* scores as $n_l^{\text{null}}(\alpha)$, in which the four corners are also randomly selected spatial points in the sample. Null scores are understood to be the score values when the four additional data points have no spatial meaning. Finally, pick α to be a value that does not exceed the first value where the two $\{n_l(\alpha), l = 1, \dots, 100\}$ and $\{n_l^{\text{null}}(\alpha), l = 1, \dots, 100\}$ are visibly separated. The first panel in Figure 2 shows an example of the “non-null” scores $n_l(\alpha)$ and null scores $n_l^{\text{null}}(\alpha)$ from the example in Section 3.1 – with a 95% balanced quantile bands shown as solid lines. This plot suggests that α values that are smaller or equal to 0.4 are values for which the spatial information (D_{geo}) has not fully *saturated* the clustering, since there was no clear separation between the scores and the null scores for $\alpha \leq 0.4$.

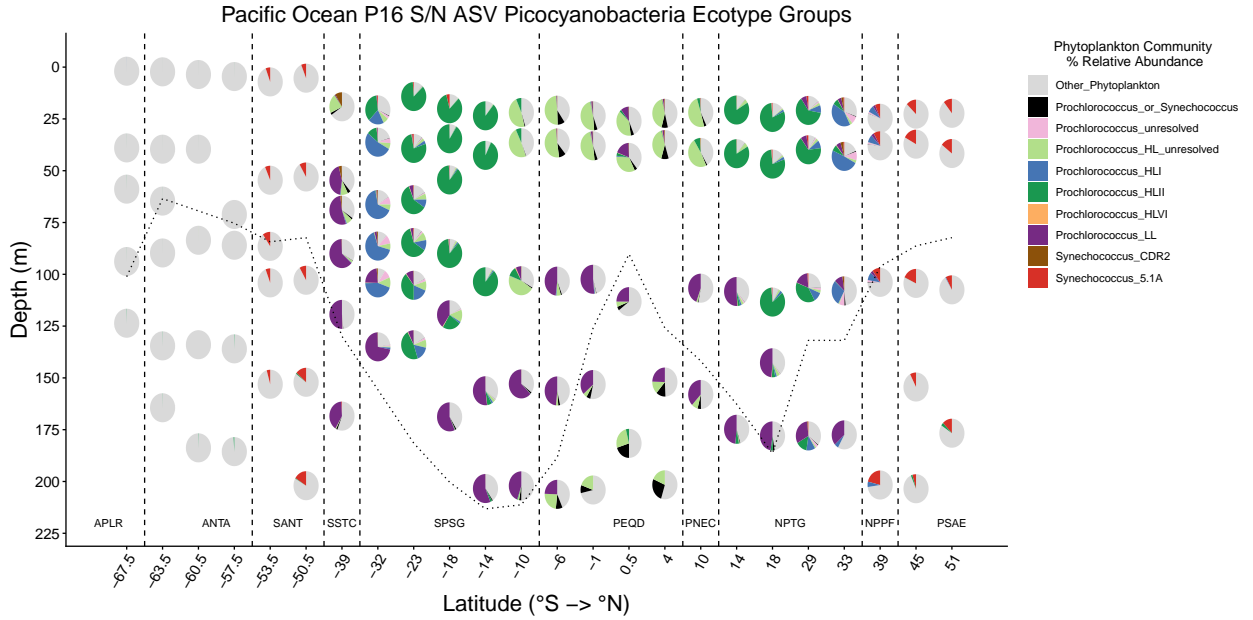


Figure 14: Vertical and spatial distribution of phytoplankton community composition across the P16 S/N transect. Each pie chart represents the aggregated relative abundance of ASVs belonging to major picocyanobacteria ecotypes in context to the residual phytoplankton ASVs including diazotrophic cyanobacteria and eukaryotic phytoplankton (derived from chloroplast 16S) colored in gray at a given sampling depth and latitude in the upper 200m along the transect. The dotted horizontal line within each station denotes the approximate lower boundary of the euphotic zone. Vertical dashed lines separate distinct biogeographical regions along the transect, annotated by Longhurst provinces.

References

- [1] Mark D. Spalding, Helen E. Fox, Gerald R. Allen, Nick Davidson, Zahra A. Ferdaña, Max A. X. Finlayson, and J. Robertson. Marine ecoregions of the world: a bioregionalization of coastal and shelf areas. *BioScience*, 57(7):573–583, 2007.
- [2] John C. Briggs and Brian W. Bowen. A realignment of marine biogeographic provinces with particular reference to fish distributions. *Journal of Biogeography*, 39(1):12–30, 2012.
- [3] Mark J. Costello, Po-Lynn Tsai, Pak-Sin Wong, Amy K. L. Cheung, Zahra Basher, and Charan Chaudhary. Marine biogeographic realms and species endemism. *Nature Communications*, 8(1):1057, 2017.
- [4] Maria T Kavanaugh, Burke Hales, Martin Saraceno, Yvette H Spitz, Angelique E White, and Ricardo M Letelier. Hierarchical and dynamic seascapes: A quantitative framework for scaling pelagic biogeochemistry and ecology. *Progress in Oceanography*, 120:291–304, 2014.
- [5] Gabriel Reygondeau, William W. L. Cheung, Colette C. C. Wabnitz, Vicky W. Y. Lam, Thomas Frölicher, and Olivier Maury. Climate change-induced emergence of novel biogeochemical provinces. *Frontiers in Marine Science*, 7, October 2020.
- [6] Alessandro Tagliabue, Lester Kwiatkowski, Laurent Bopp, Momme Butenschön, William Cheung, Matthieu Lengaigne, and Jerome Vialard. Persistent uncertainties in ocean net primary production climate change projections at regional scales raise challenges for assessing impacts on ecosystem services. *Frontiers in Climate*, 3, November 2021.
- [7] Jordan Winter, Annette Hynes, Chris Berthiaume, Kelsy Cain, E. Virginia Armbrust, and François Ribaut. Shifts in phytoplankton community structure across oceanic boundaries. *PLOS ONE*, 20(6):1–16, 06 2025.
- [8] Cora Hörstmann, Pier Luigi Buttigieg, Uwe John, Eric J Raes, Dieter Wolf-Gladrow, Astrid Bracher, and Anya M Waite. Microbial diversity through an oceanographic lens: refining the concept of ocean provinces through trophic-level analysis and productivity-specific length scales. *Environmental microbiology*, 24(1):404–419, 2022.
- [9] Eric J. Raes, Levente Bodrossy, Jodie van de Kamp, Andrew Bissett, Martin Ostrowski, Mark V. Brown, Swan L. S. Sow, Bernadette Slovan, and Anya M. Waite. Oceanographic boundaries constrain microbial diversity gradients in the south pacific ocean. *Proceedings of the National Academy of Sciences*, 115(35), August 2018.
- [10] MLD Palomares, Rainer Froese, B Derrick, JJ Meeuwig, S-L Noël, G Tsui, J Woroniak, D Zeller, and D Pauly. Fishery biomass trends of exploited fish populations in marine ecoregions, climatic zones and ocean basins. *Estuarine, Coastal and Shelf Science*, 243:106896, 2020.
- [11] Marit van Oostende, Martin Hieronymi, Hajo Krasemann, and Burkard Baschek. Global ocean colour trends in biogeochemical provinces. *Frontiers in Marine Science*, 10, May 2023.
- [12] Marcello Vichi, J. Icarus Allen, Simona Masina, and Nicholas J. Hardman-Mountford. The emergence of ocean biogeochemical provinces: A quantitative assessment and a diagnostic for model evaluation: Model assessment of ocean provinces. *Global Biogeochemical Cycles*, 25(2), May 2011.
- [13] Maike Sonnewald, Stephanie Dutkiewicz, Christopher Hill, and Gael Forget. Elucidating ecological complexity: Unsupervised learning determines global marine eco-provinces. *Science advances*, 6(22):eaay4740, 2020.
- [14] Shubha Sathyendranath, Alan Longhurst, Cathy M. Caverhill, and Trevor Platt. Regionally and seasonally differentiated primary production in the north atlantic. *Deep Sea Research Part I: Oceanographic Research Papers*, 42(10):1773–1802, 1995.

- [15] Alan Longhurst, Shubha Sathyendranath, Trevor Platt, and Cathy Caverhill. An estimate of global primary production in the ocean from satellite radiometer data. *Journal of Plankton Research*, 17(6):1245–1271, 1995.
- [16] A.R. Longhurst. *Ecological Geography of the Sea*. Academic Press, 01 2007.
- [17] Stanford B. Hooker, Nigel W. Rees, and James Aiken. An objective methodology for identifying oceanic provinces. *Progress in Oceanography*, 45(3-4):313–338, 2000.
- [18] Matthew J. Oliver and Andrew J. Irwin. Objective global ocean biogeographic provinces. *Geophysical Research Letters*, 35(15), 2008.
- [19] Gabriel Reygondeau, Alan Longhurst, Emmanuel Martinez, Grégory Beaugrand, David Antoine, and Olivier Maury. Dynamic biogeochemical provinces in the global ocean. *Global Biogeochemical Cycles*, 27(4):1046–1058, 2013.
- [20] Tracey T. Sutton, Malcolm R. Clark, Daniel C. Dunn, Patrick N. Halpin, Alex D. Rogers, John Guinotte, and M. Heino. A global biogeographic classification of the mesopelagic zone. *Deep Sea Research Part I: Oceanographic Research Papers*, 126:85–102, 2017.
- [21] Urdanibia H. Elizondo, D. Righetti, F. Benedetti, and M. Vogt. Biome partitioning of the global ocean based on phytoplankton biogeography. *Progress in Oceanography*, 194:102530, 2021.
- [22] Carlos M. Duarte. Seafaring in the 21st century: the malaspina 2010 circumnavigation expedition, 2022.
- [23] Shinichi Sunagawa et al. Tara oceans: towards global ocean ecosystems biology. *Nature Reviews Microbiology*, 18(8):428–445, 2020.
- [24] Jesse McNichol, Paul M. Berube, Steven J. Biller, and Jed A. Fuhrman. Evaluating and improving small subunit rna pcr primer coverage for bacteria, archaea, and eukaryotes using metagenomes from global ocean surveys. *mSystems*, 6(3):10–1128, 2021.
- [25] Fabrice Vincent, F. M. Ibarbalz, and Chris Bowler. Global marine phytoplankton revealed by the tara oceans expedition. In *Advances in Phytoplankton Ecology*, pages 531–561. Elsevier, 2022.
- [26] Felix Milke, Jan Meyerjürgens, and Meinhard Simon. Ecological mechanisms and current systems shape the modular structure of the global oceans’ prokaryotic seascape. *Nature Communications*, 14(1):6141, 2023.
- [27] Jesse McNichol, Nathan L. R. Williams, Yubin Raut, Craig Carlson, Elisa R. Halewood, Kendra Turk-Kubo, Jonathan P. Zehr, Andrew P. Rees, Glen Tarran, Mary R. Gradoville, Matthias Wietz, Christina Bienhold, Katja Metfies, Sinhué Torres-Valdés, Thomas Mock, Sarah Lena Eggers, Wade Jeffrey, Joseph Moss, Paul Berube, Steven Biller, Levente Bodrossy, Jodie Van De Kamp, Mark Brown, Swan L. S. Sow, E. Virginia Armbrust, and Jed Fuhrman. Characterizing organisms from three domains of life with universal primers from throughout the global ocean. *Scientific Data*, 12(1):1078, July 2025.
- [28] Stephanie Dutkiewicz, Christopher L. Follett, Michael J. Follows, Fernanda Henderikx-Freitas, Francois Ribalet, Mary R. Gradoville, Sacha N. Coesel, Hanna Farnelid, Zoe V. Finkel, Andrew J. Irwin, Oliver Jahn, David M. Karl, Jann Paul Mattern, Angelique E. White, Jonathan P. Zehr, and E. Virginia Armbrust. Multiple biotic interactions establish phytoplankton community structure across environmental gradients. *Limnology and Oceanography*, 69:1086–1100, 2024.
- [29] Alma E Parada, David M Needham, and Jed A Fuhrman. Every base matters: assessing small subunit rna primers for marine microbiomes with mock communities, time series and global field samples. *Environmental microbiology*, 18(5):1403–1414, 2016.
- [30] Paul G Falkowski, Richard T Barber, and Victor Smetacek. Biogeochemical controls and feedbacks on ocean primary production. *science*, 281(5374):200–206, 1998.

- [31] Christopher B Field, Michael J Behrenfeld, James T Randerson, and Paul Falkowski. Primary production of the biosphere: integrating terrestrial and oceanic components. *science*, 281(5374):237–240, 1998.
- [32] Richard G. Dorrell and Christopher J. Howe. What makes a chloroplast? reconstructing the establishment of photosynthetic symbioses. *Journal of Cell Science*, January 2012.
- [33] V. Lila Koumandou, R. Ellen R. Nisbet, Adrian C. Barbrook, and Christopher J. Howe. Dinoflagellate chloroplasts – where have all the genes gone? *Trends in Genetics*, 20(5):261–267, May 2004.
- [34] J. Aitchison. The statistical analysis of compositional data. *Journal of the Royal Statistical Society: Series B (Methodological)*, 44(2):139–160, 01 1982.
- [35] Marie Chavent, Vanessa Kuentz-Simonet, Amaury Labenne, Jérôme Saracco, Marie Chavent, Vanessa Kuentz-Simonet, Amaury Labenne, and Jérôme Saracco. Clustgeo: an r package for hierarchical clustering with spatial constraints. *Computational Statistics 2018 33:4*, 33(4), 2018-01-20.
- [36] Robert R. Sokal and Charles D. Michener. A statistical method for evaluating systematic relationships. *University of Kansas Science Bulletin*, 38(22):1409–1438, 1958.
- [37] Joe H. Ward. Hierarchical grouping to optimize an objective function. *Journal of the American Statistical Association*, 58(301):236–244, March 1963.
- [38] Jeffrey C. Nekola and Peter S. White. The distance decay of similarity in biogeography and ecology. *Journal of Biogeography*, 26(4):867–878, July 1999.
- [39] R. T. Barber, M. P. Sanderson, S. T. Lindley, F. Chai, J. Newton, C. C. Trees, and F. P. Chavez. Primary productivity and its regulation in the equatorial pacific during and following the 1991–1992 El Niño. *Deep Sea Research Part II: Topical Studies in Oceanography*, 43(4-6):933–969, 1996.
- [40] Richard T. Barber and Francisco P. Chavez. Regulation of primary productivity rate in the equatorial Pacific. *Limnology and Oceanography*, 36(8):1803–1815, 1991.
- [41] Richard C. Dugdale and Frances P. Wilkerson. Silicate regulation of new production in the equatorial Pacific upwelling. *Nature*, 391(6664):270–273, 1998.
- [42] Michael. C. G. Carlson, François Ribalet, Ilia Maidanik, Bryndan P. Durham, Yotam Hulata, Sara Ferrón, Julia Weissenbach, Nitzan Shamir, Svetlana Goldin, Nava Baran, B. B. Cael, David M. Karl, Angelique E. White, E. Virginia Armbrust, and Debbie Lindell. Viruses affect picocyanobacterial abundance and biogeography in the north pacific ocean. *Nature Microbiology*, 7(4):570–580, April 2022.
- [43] Christopher L. Follett, Stephanie Dutkiewicz, François Ribalet, Emily Zakem, David Caron, E. Virginia Armbrust, and Michael J. Follows. Trophic interactions with heterotrophic bacteria limit the range of prochlorococcus. *Proceedings of the National Academy of Sciences*, 119(2), January 2022.
- [44] André Morel, Hervé Claustre, and Bernard Gentili. The most oligotrophic subtropical zones of the global ocean: similarities and differences in terms of chlorophyll and yellow substance. *Biogeosciences*, 7(10):3139–3151, 2010.
- [45] Pedro Flombaum, José L. Gallegos, Rodolfo A. Gordillo, José Rincón, Lina L. Zabala, Nianzhi Jiao, David M. Karl, William K. W. Li, Michael W. Lomas, Daniele Veneziano, Carolina S. Vera, Jasper A. Vrugt, and Adam C. Martiny. Present and future global distributions of the marine Cyanobacteria Prochlorococcus and Synechococcus. *Proceedings of the National Academy of Sciences*, 110(24):9824–9829, 2013.
- [46] Zackary I Johnson, Erik R Zinser, Allison Coe, Nathan P McNulty, E Malcolm S Woodward, and Sallie W Chisholm. Niche partitioning among prochlorococcus ecotypes along ocean-scale environmental gradients. *Science*, 311(5768):1737–1740, 2006.

- [47] Steven J Biller, Paul M Berube, Debbie Lindell, and Sallie W Chisholm. Prochlorococcus: the structure and function of collective diversity. *Nature Reviews Microbiology*, 13(1):13–27, 2015.
- [48] Walker O Smith Jr and Randolph M Jones. Vertical mixing, critical depths, and phytoplankton growth in the ross sea. *ICES Journal of Marine Science*, 72(6):1952–1960, 2015.
- [49] Diana Zúñiga, Anna Sanchez-Vidal, María del Mar Flexas, Dustin Carroll, Marta M Rufino, Gunnar Spreen, Antoni Calafat, and Fátima Abrantes. Sinking diatom assemblages as a key driver for deep carbon and silicon export in the scotia sea (southern ocean). *Frontiers in Earth Science*, 9:579198, 2021.
- [50] Natalie R Cohen, Matthew R McIlvin, Dawn M Moran, Noelle A Held, Jaclyn K Saunders, Nicholas J Hawco, Michael Brosnahan, Giacomo R DiTullio, Carl Lamborg, John P McCrow, et al. Dinoflagellates alter their carbon and nutrient metabolic strategies across environmental gradients in the central pacific ocean. *Nature Microbiology*, 6(2):173–186, 2021.